Evaluating a topo-bathymetric lidar sensor to map Submerged Aquatic Vegetation in Lake Banook

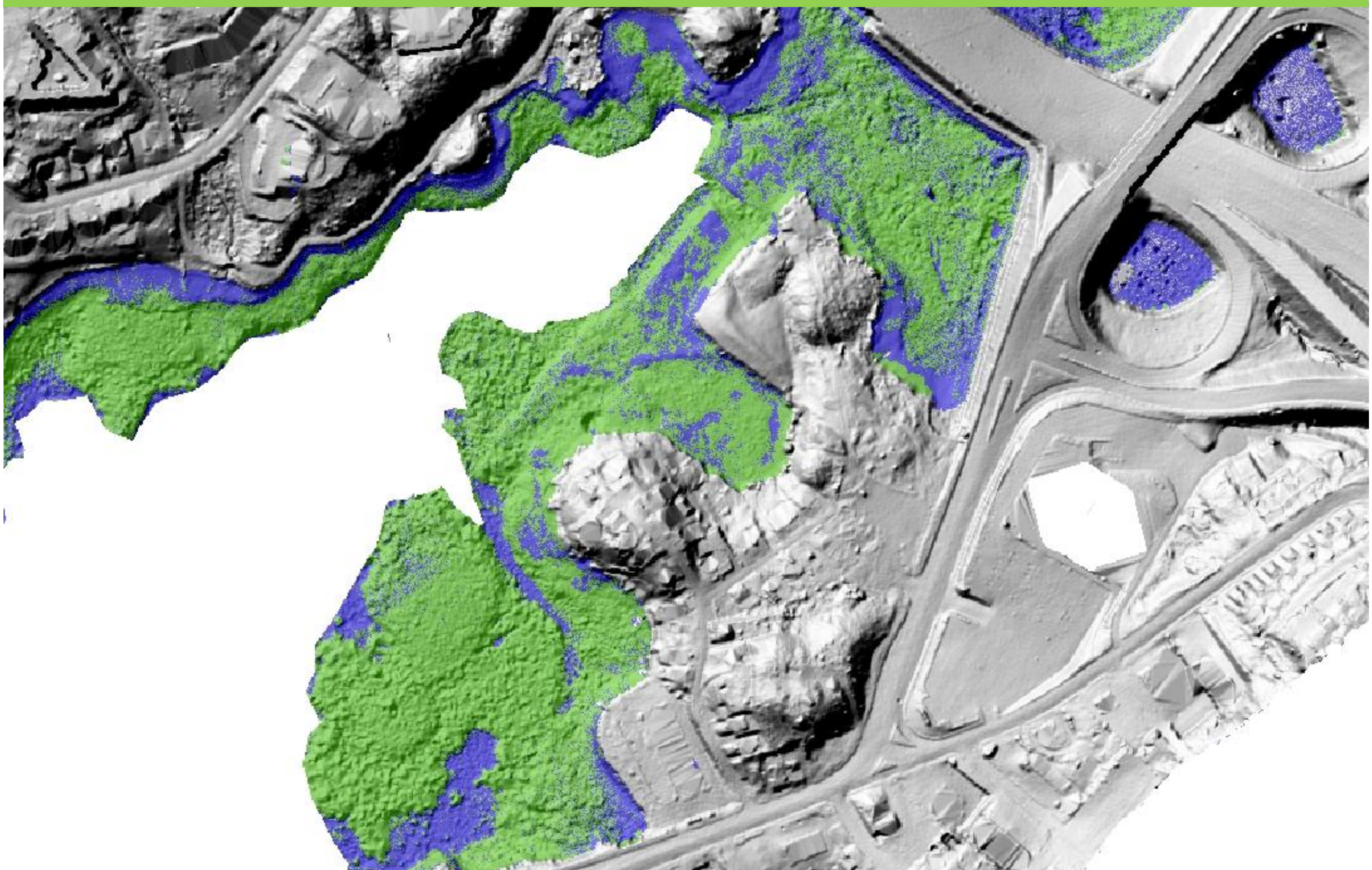

Prepared by

Tim Webster, PhD
Kevin McGuigan, Kate Collins,
Nathan Crowell, Candace MacDonald
Applied Geomatics Research Group
NSCC, Middleton
Tel. 902 825 5475
email: tim.webster@nscc.ca

Submitted to

Elizabeth Kennedy
Stantec Consulting Ltd.

April 27, 2015

How to cite this work and report:

Webster, T., McGuigan, K., Collins, K., Crowell, N., MacDonald, C. 2015. Evaluating a topo-bathymetric lidar sensor to map Submerged Aquatic Vegetation in Lake Banook. Technical report, Applied Geomatics Research Group, NSCC Middleton, NS.

Copyright and Acknowledgement

The Applied Geomatics Research Group of the Nova Scotia Community College maintains full ownership of all data collected by equipment owned by NSCC and agrees to provide the end user who commissions the data collection a license to use the data for the purpose they were collected for upon written consent by AGRG-NSCC. The end user may make unlimited copies of the data for internal use; derive products from the data, release graphics and hardcopy with the copyright acknowledgement of **"Data acquired and processed by the Applied Geomatics Research Group, NSCC"**. Data acquired using this technology and the intellectual property (IP) associated with processing these data are owned by AGRG/NSCC and data will not be shared without permission of AGRG/NSCC.

Executive Summary

An airborne topographic-bathymetric lidar survey was undertaken at Lake Banook, Dartmouth Nova Scotia on September 24, 2014. The focus of the study was to test the limitations of the lidar sensor for the application of monitoring submerged aquatic vegetation (SAV) distribution and biomass in a lake environment. The sensor used was a Chiroptera II integrated topographic bathymetric lidar sensor equipped with a 60 megapixel multispectral camera. Ground truth data was collected during the aerial survey and included depth, Secchi depth, and turbidity measurements. Conditions during the survey were calm and clear but followed a storm of high wind and rain on September 22. The aircraft used ground-based high precision GPS data from a permanent Nova Scotia High Precision Network monument set up nearby.

Standard data products generated included a digital elevation model (DEM), digital surface model (DSM), and lidar reflectance grid all with 1 m resolution, and an aerial orthophoto mosaic at 20 cm resolution. New and innovative techniques were developed to classify SAV that encompassed multiple components of the data obtained during the aerial survey including the reflectance, aerial photographs, and bathymetry data. The method involved normalizing the reflectance data and aerial photographs for depth, classifying SAV using a threshold value for each layer, and combining each layer using a weighted approach.

The map of SAV presence/absence agreed with our ground truth data with more than 80% accuracy. Successful laser penetration was limited to 4.5 m depth by a combination of turbidity and depth itself, which sharply dropped off in many dredged and steep-sided areas of the lake. The SAV map was spatially limited to the areas where laser penetrated to the bottom of the lakebed but within the area of good bathymetric data returns we were able to successfully classify SAV. Of the area that we classified (32.32 hectares) , 54.9% of the area contained SAV (17.74 hectares), which varied in height from less than 0.1 m to 1.88 m.

Table of Contents

Table of Figures

List of Tables

1 Introduction

Lake Banook, located in urban Dartmouth, Nova Scotia (Figure 1.1), is a popular lake for recreational and international-level paddlers, swimmers, and home-owners, but has been plagued recently by excessive pondweed growth. A report commissioned by the Halifax Regional Municipality (HRM) found that the weeds are native to the area, but lowered lake levels in 2009 combined with sediment enrichment from non-point source urban sediment loading, triggered a growth spurt that has gone unchecked and is hindering users of the lake (Stantec, 2014). The report suggests several different remediation options to control the weed, such as management of storm water infrastructure or chemically eliminating the weed. The report concludes, however, that quantitative biomass monitoring before any weed control methods are undertaken is essential, followed by yearly biomass monitoring to confirm the effectiveness of the vegetation control (Stantec, 2014).

The Nova Scotia Community College's Applied Geomatics Research Group (NSCC-AGRG) was awarded funding by the National Science and Engineering Research Council (NSERC) to work with Stantec on the issue of weed mapping, monitoring, and quantification. NSCC has a newly obtained topographic-bathymetric (topo-bathy) lidar sensor that is capable of surveying the land elevations and submerged lake topography using a laser ranging system onboard an aircraft. The research goal of this project was to investigate the lidar sensor's ability to map the distribution and density of the submerged vegetation. If successful, the topo-bathy lidar sensor would be an effective tool for repeat biomass monitoring surveys of Lake Banook, and would prove the technology can be used for this application in other lakes. A benefit of the topo-bathy lidar system is the number of valuable datasets obtained during just one survey: a digital elevation model (DEM) of the lake bathymetry, high resolution orthophoto mosaic, and a map of the distribution of the weed. The combination of these data products can provide new information on the spatial distribution of the weed in three dimensions.

1.1 Study Area

Lake Banook is an urban lake in central Dartmouth only 1.5 km from Halifax Harbour, and is the last lake in the historic Shubenacadie Canal (Figure 1.1). The lake is 1.3 km long, 500 m wide, and 11 m deep (Huppertz et al., 2008a). Land use along the lakeshore includes residential (homes and condominiums), commercial (including the nearby MicMac Mall), roadways (including the busy Highway 111), and recreational (canoe clubs have been established on the lake since 1903).

The lake has seen many modifications to its shoreline and bathymetry, both anthropogenic and geologic. Scientists from the Geological Survey of Canada (GSC) conducted a geophysical survey of the lake in 2007 to collect multibeam bathymetry, sidescan sonar, seismic, and underwater video data (Huppertz et al., 2008a; King et al., 2007). As part of the Shubenacadie Canal construction in the 1850s the lake was dammed, causing an island to be submerged and the lake level to rise by several meters; Huppertz et al. (2008a) identify this pre-canal natural shoreline in their multibeam data as terraces in the lake characterized by variation in boulder density and rapid changes in depth. King et al. (2007) also identified a paleo-shoreline and paleo-riverbeds that predate the Shubenacadie Canal construction. The analysis of the GSC Banook data showed dredged and slumped areas, classified the lakebed material, and analyzed the seismic data below the lakebed to identify numerous geological evolution events including deglaciation and lake flooding (Huppertz et al., 2008a; King et al., 2007). Anthropogenic changes to the bathymetry have occurred on numerous occasions. The lake has been drained or lowered at least four times (1969, 1976, 1997, 2008) (Canada Games, 2015; Gordon, 1978; Stantec, 2014; Halifax Regional Municipality, 2008) and dredged at least twice (1976, 1997) (Gordon, 1978; Stantec, 2014). The geological and anthropogenic bathymetry and shoreline changes such as submerged and removed islands, and dredged areas are discussed and explored using the lidar bathymetry data in the Discussion section.

Figure 1.1: Lake Banook and the bathymetric lidar study area, which included the southern tip of Lake MicMac and Sullivan's Pond.

1.2 Water Clarity

Bathymetric lidar is limited by water clarity, which is related to turbidity, the amount of light scattered by particles in the water column. Turbid water can be caused by silt, suspended sediment, bacteria, algae, or humic acid. Water clarity is commonly measured using a Secchi disk, a black and white disk that is lowered into the water to determine the depth of light penetration, while turbidity is measured by measuring the amount of light scattered off suspended particles using a turbidity meter.

Lake Banook has been well-studied over the years and a wealth of water quality data exist on the lake (Castell, 1977; Gordon, 1973, 1978; Huppertz et al., 2008b; Wyre, 2006). The lake has been part of a long-term study of ~50 lakes in the HRM conducted by Fisheries and Oceans Canada (DFO) called the Synoptic Water Quality Survey. Once a year, the lakes were sampled and several water quality variables were measured such as pH, conductivity, nutrients, and elements. Lake Banook was surveyed as part of this study in 1980, 1991, 2000, and 2011, although the 2011 results have not yet been published (Gordon et al., 1981; Keizer et al., 1993; Clement et al., 2007). The HRM Lakes Water Quality Monitoring Program was conducted between 2006 and 2011 and measured selected water quality variables three times a year, and most recently, Stantec (2014) conducted similar measurements in November 2013 for their study of the lake weeds. The Stantec report presents a table summarizing the data available from each of these studies. Secchi depths ranged from 2.0 m (spring 2009) to 7.4 m (fall 2010), turbidity ranged from 0.5 NTU (summer 2007 and 2009, and fall 2008) to 1.2 NTU (summer 2010). Of the 51 lakes sampled by DFO in 2000 Banook had the lowest value for lake colour, as measured based on dissolved organic carbon (DOC) in true colour units (TCU); in the HRM fall 2011 Banook had the lowest colour of the 52 lakes sampled. The trophic status index (TSI) for Banook was about average at ~35 in 1991 and 2000, where a TSI > 50 indicates eutrophic conditions.

The DFO (2007) report emphasizes that major wind and precipitation events have a pronounced effect on lake water quality. Gordon (1973) noted that very fine sediment grains in Lake Banook remained suspended in the water column even as the water moved over large distances, and Castell (1977) found that wave action re-suspended bottom sediments that had accumulated following a lowering of Lake MicMac in 1977. Wyre (2006) studied suspended sediment in Lake MicMac during heavy rainfall events in the fall of 2005 and found very high silt and clay sediment washed into the lake as runoff but was associated with a construction site that later improved their water retention methods and concentrations of sediments entering the lake system during subsequent rainfall events were reduced. In their report, Stantec (2014) sampled “wet” and “dry” conditions during November 2013 and found an increase in total suspended solids at the stream location nearest the mall, while the other sampled locations showed no change.

2 Methods

2.1 Sensor Specifications and Installation

The lidar sensor is a Chiroptera II integrated topographic bathymetric lidar sensor equipped with a 60 megapixel multispectral camera. The system incorporates a 1064 nm near infrared (NIR) laser for ground returns and sea surface and a green 532 nm laser for bathymetric returns (Figure 2.1). The lasers scan in an elliptical pattern, which enables coverage from many different angles, on vertical faces, causes less shadow effects in the data, and is less sensitive to wave interaction. The bathymetric laser is limited by depth and clarity, and has a depth penetration rating of 1.5 x the Secchi depth. The Leica RCD30 camera collects co-aligned RGB (red, green, blue) + NIR motion compensated photographs which can be mosaicked into a single image in post-processing, or analyzed frame by frame for maximum information extraction.

AGRG-NSCC does not own an aircraft, only the sensor. AGRG partnered with Leading Edge Geomatics to assist in the operations of the survey and arranging the aircraft. A twin engine aircraft was contracted that was certified to carry the Chiroptera II sensor suite and had a hole suitable to house the sensor head. The lidar sensor was installed in the aircraft in Fredericton, NB on Sept. 22. Calibration flights were conducted over Fredericton at altitudes of 400 m and 1000 m on Sept. 23. The laser systems and camera were calibrated and aligned with the navigation system which consists of a survey grade global positioning system (GPS) mounted on the roof of the aircraft and an inertial measurement unit (IMU) mounted above the laser system (Figure 2.2.)

The aircraft had a hole cut in the bottom for the laser to face the ground and installation involved fitting the control unit and the sensor head into the hole (Figure 2.2b). The system also includes a 5 megapixel quality assurance camera that the lidar operator is able to view during the flight, along with the waveform of the returning pulse and the flight plan (Figure 2.2c). Figure 2.2d shows the downward facing portion of the sensor head, including the red (topographic) and green (bathymetric) lasers, which shoot and return to the large red circles; the lenses on the left and right are the low and high resolution cameras, respectively.

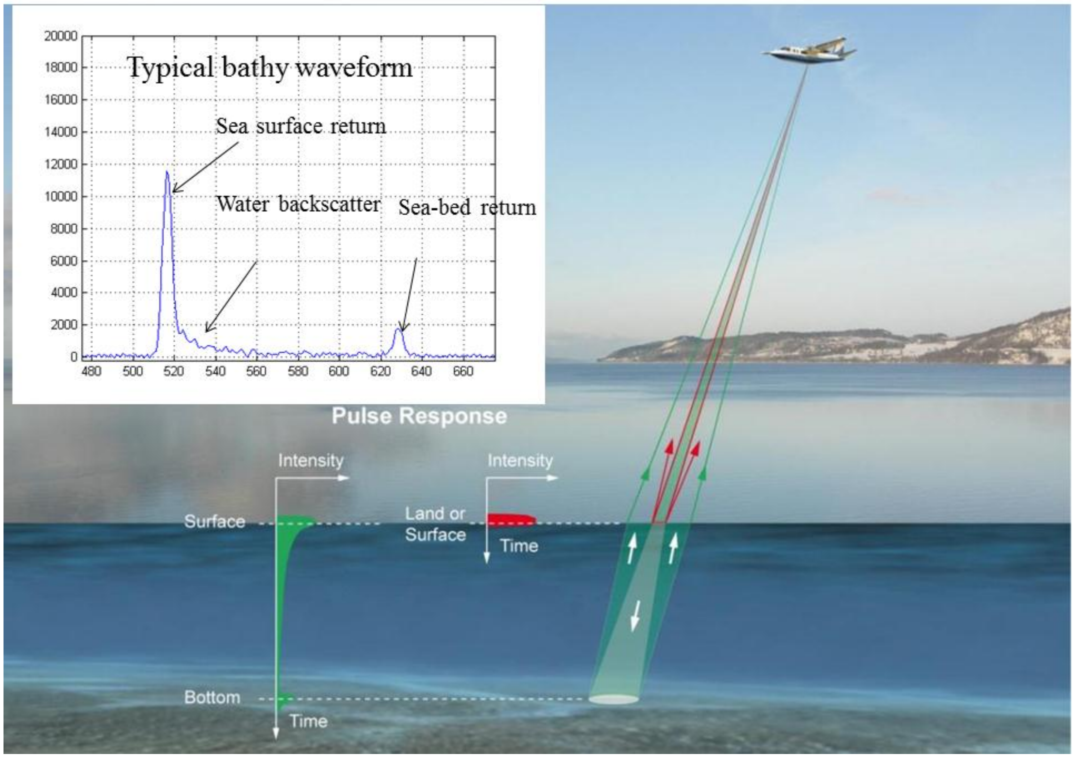

Figure 2.1: Principals of topo-bathymetric lidar. The system utilizes two lasers, a near infrared and a green laser to surface the land and marine topography.

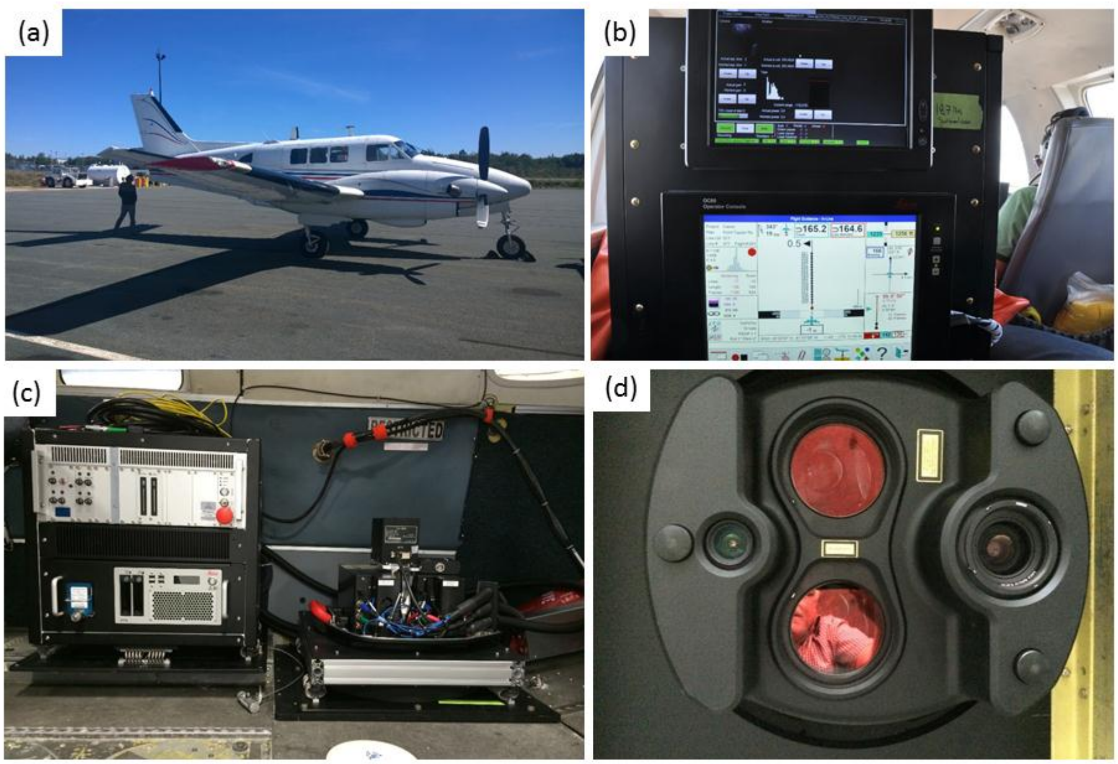

Figure 2.2: (a) Aircraft used for September 2014 lidar survey; (b) display seen by lidar operator in-flight; (c) main body of sensor (left) and laser pointing through a hole cut in the bottom of the plane (right); (d) large red circles are the lasers; the RCD30 lens (right) and low resolution camera (left).

2.2 Meteorological Conditions

Meteorological conditions during and prior to topo-bathy lidar data collection are an important factor in successful data collection. As the lidar sensor is limited by water clarity, windy weather has the potential to stir up any fine sediment in the water and prevent good laser penetration, and precipitation can flush sediment into the water via rivers or culverts. Rainy weather is not suitable for lidar collection, and the glare of the sun must also be factored in for the collection of aerial photography. Before the lidar survey we monitored weather forecasts, current and past conditions using the closest weather station to the Lake Banook study site, which is operated by Environment Canada at Halifax, NS (Figure 2.3). Local knowledge of the water clarity in a bathymetric lidar survey study area is critical, as some areas are more susceptible to wind or rain-induced turbidity. We referred to the seasonal turbidity data for Lake Banook compiled in the Stantec report (2014) and also communicated with Stantec directly to learn that the sediment in Lake Banook is not prone to being stirred up by wind, and winds should not pose a significant threat; but the lake can experience suspended sediments due to runoff following rainfall, as discussed in Section 1.2. A strong wind and rain event on Sept. 22 (Figure 2.4) brought strong winds and rain to much of the province and put much of our coastal surveying on hold for several days, but a visual check of the lake on the morning of the survey showed that any ill-effects from the storm in Lake Banook appeared to have cleared up by Sept. 24, which was a clear day with light winds.

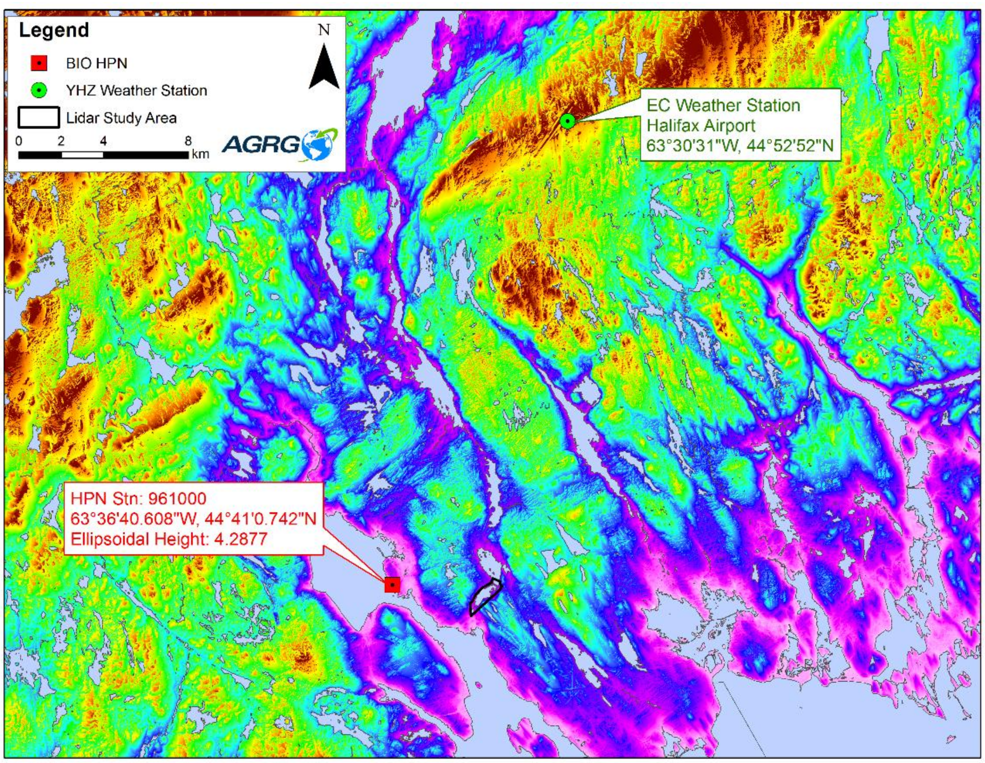

Figure 2.3: Locations of the HPN station used during the lidar survey and the Environment Canada weather station.

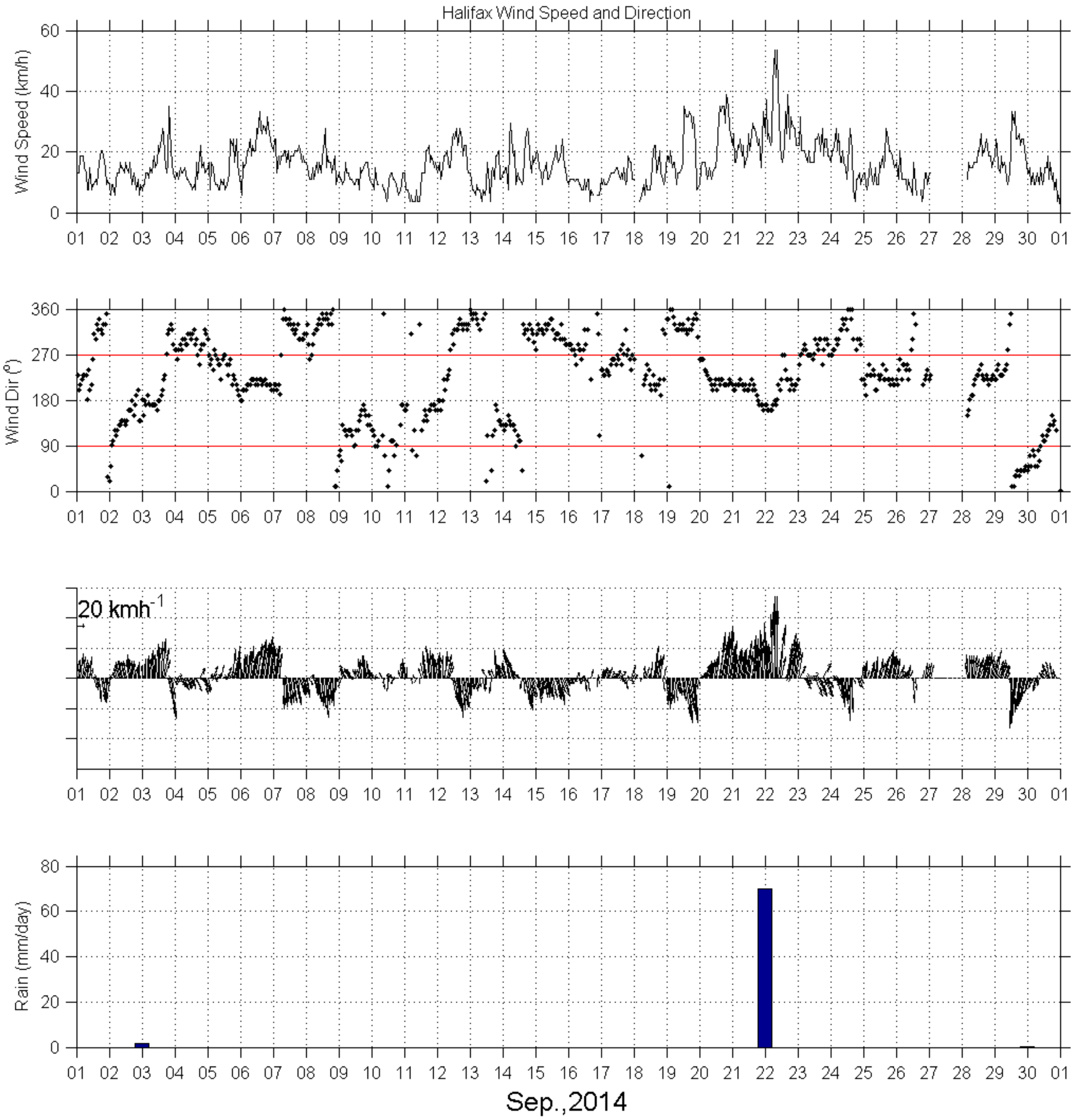

Figure 2.4: Wind speed (top panel) and direction (second panel) collected at the EC weather station at Halifax between September 1 and October 1, 2014 at 1 hour intervals. The third panel shows a vector plot of the wind, where the arrows point in the direction the wind is blowing; the bottom panel shows daily precipitation (mm).

2.3 Lidar Survey Details

The lidar survey was conducted on the morning of Wednesday, Sept. 24. The planned flight lines are shown in Figure 2.5. The aircraft required ground-based high precision GPS data to be collected during the lidar survey in order to provide accurate positional data for the aircraft trajectory. We accessed data from a permanent GPS base station set up at the Bedford Institute of Oceanography (Figure 2.3) over a Nova Scotia High Precision Network (HPN) monument. The GPS base station was set to log observations at 1 second intervals

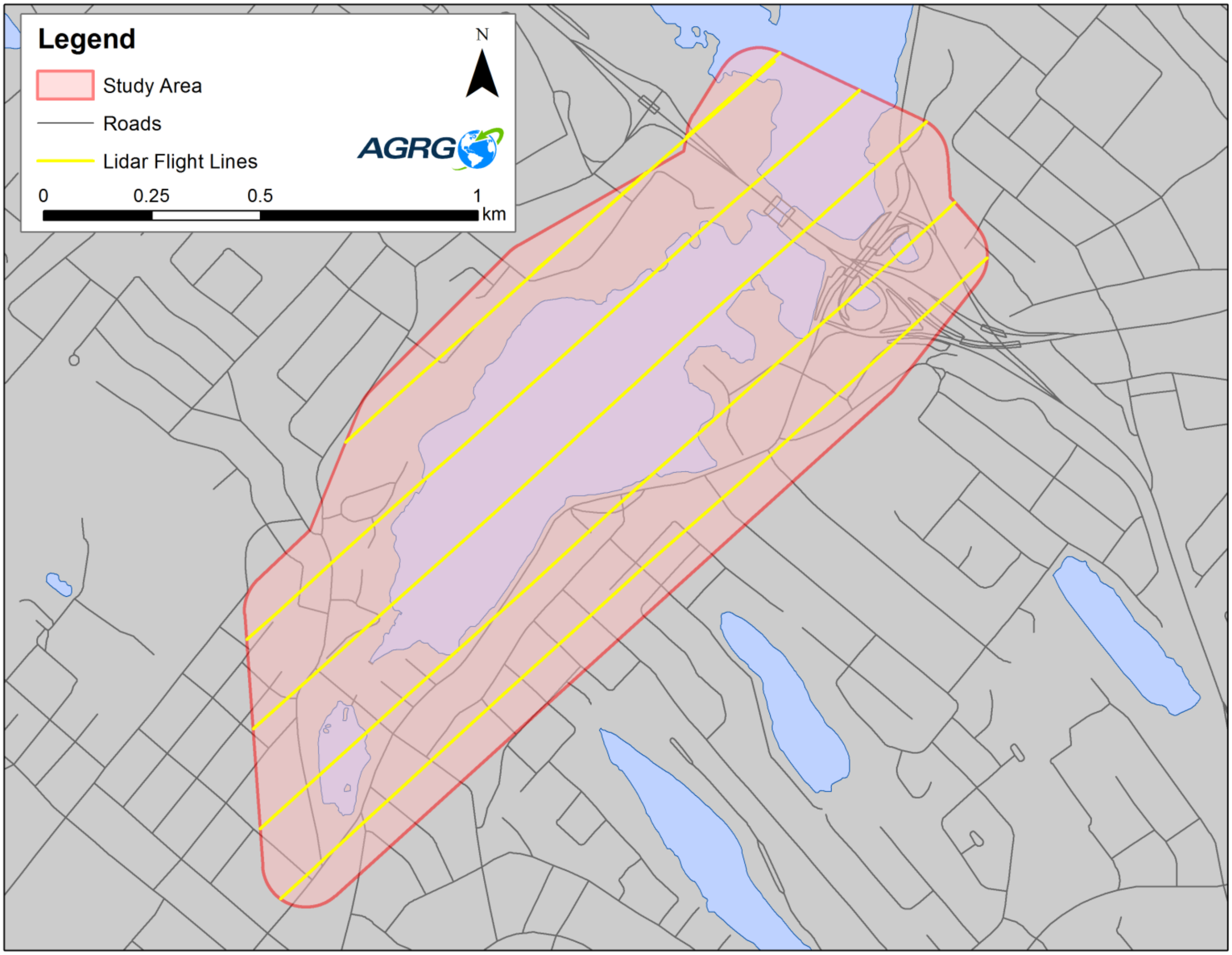

Figure 2.5: Planned lidar flight lines and polygon representing the study area.

2.4 Ground Truth Data Collection

Ground truth data is another important aspect of topo-bathy lidar data collection. In Lake Banook we conducted ground truth data collection on the day of the lidar flight, Sept. 24, with our Stantec partners. Using Stantec's small aluminum boat, we took randomly distributed measurements of depth using a lead ball and a single-beam echo sounder, Secchi depth, and turbidity (Figure 2.6). Stantec was responsible for the turbidity measurements, which were completed at several depths where water depth allowed and just at the surface otherwise. A Garmin GPS handheld unit was used to track positional data and waypoints. As part of their in-kind contribution to the project, Stantec shared a few underwater photos to assist in ground truthing that were obtained in November 2013, and bottom type information obtained on Sept. 9, 2014. Ground truth collection and coverage are summarized in Table 1 and Figure 2.7, respectively.

Table 1: Ground truth data summary.

Date	Base station for aircraft	GPS on boat	Secchi	Turbidity	Depth	Vegetation presence/absence	Percent plant cover
Sept 24, 2014	NS HPN at BIO	Garmin; AGRG	AGRG	Stantec	Lead ball, sonar; AGRG	AGRG (where visible)	
Sept 9, 2014		Stantec				Stantec	Stantec

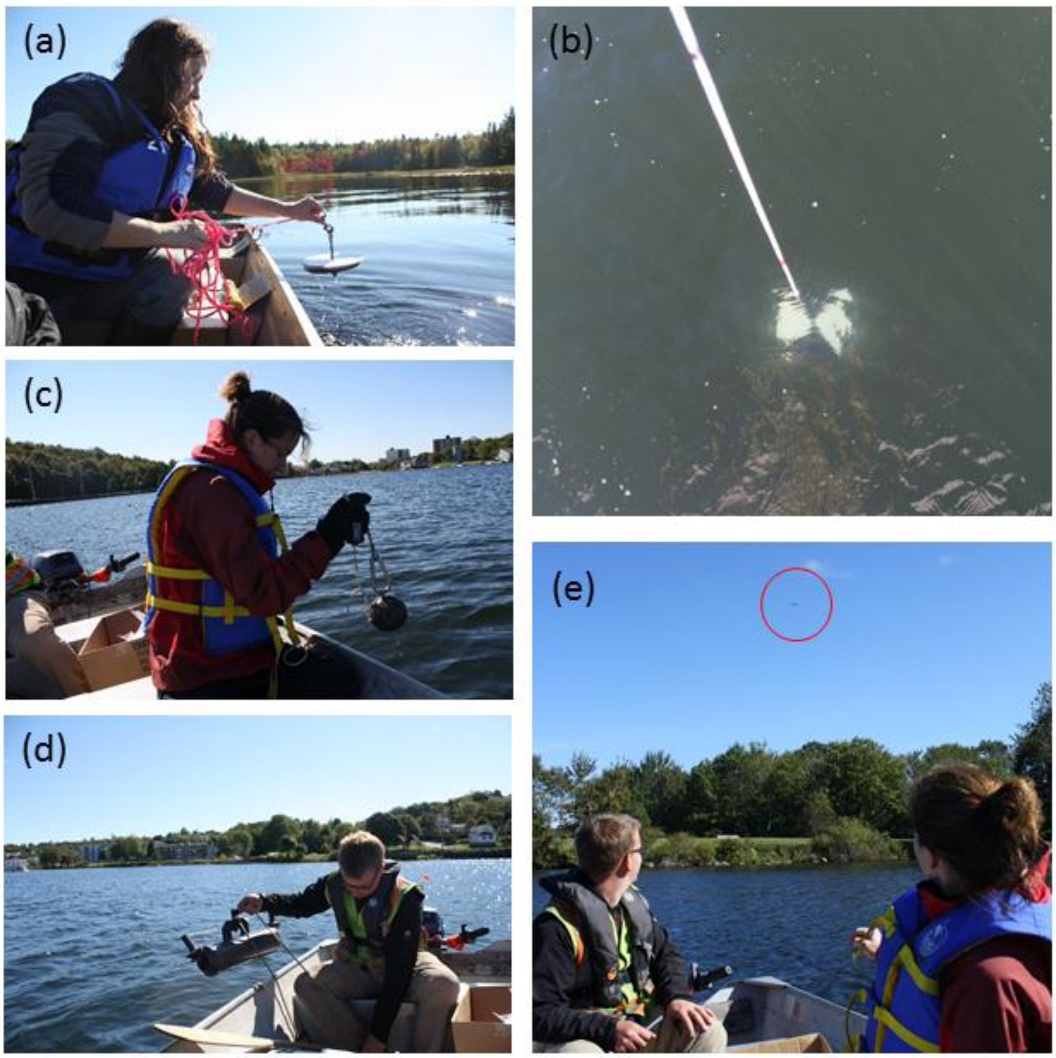

Figure 2.6: (a) AGRG researcher deploying the Secchi disk used to measure water clarity during the lidar survey with graduated rope; (b) submerged Secchi disk; (c) AGRG researcher using the lead ball for a depth measurment; (d) Stantec employee preparing to deploy the Niskin water sample bottle to measure turbidity; (e) the aircraft surveying the lake (red circle).

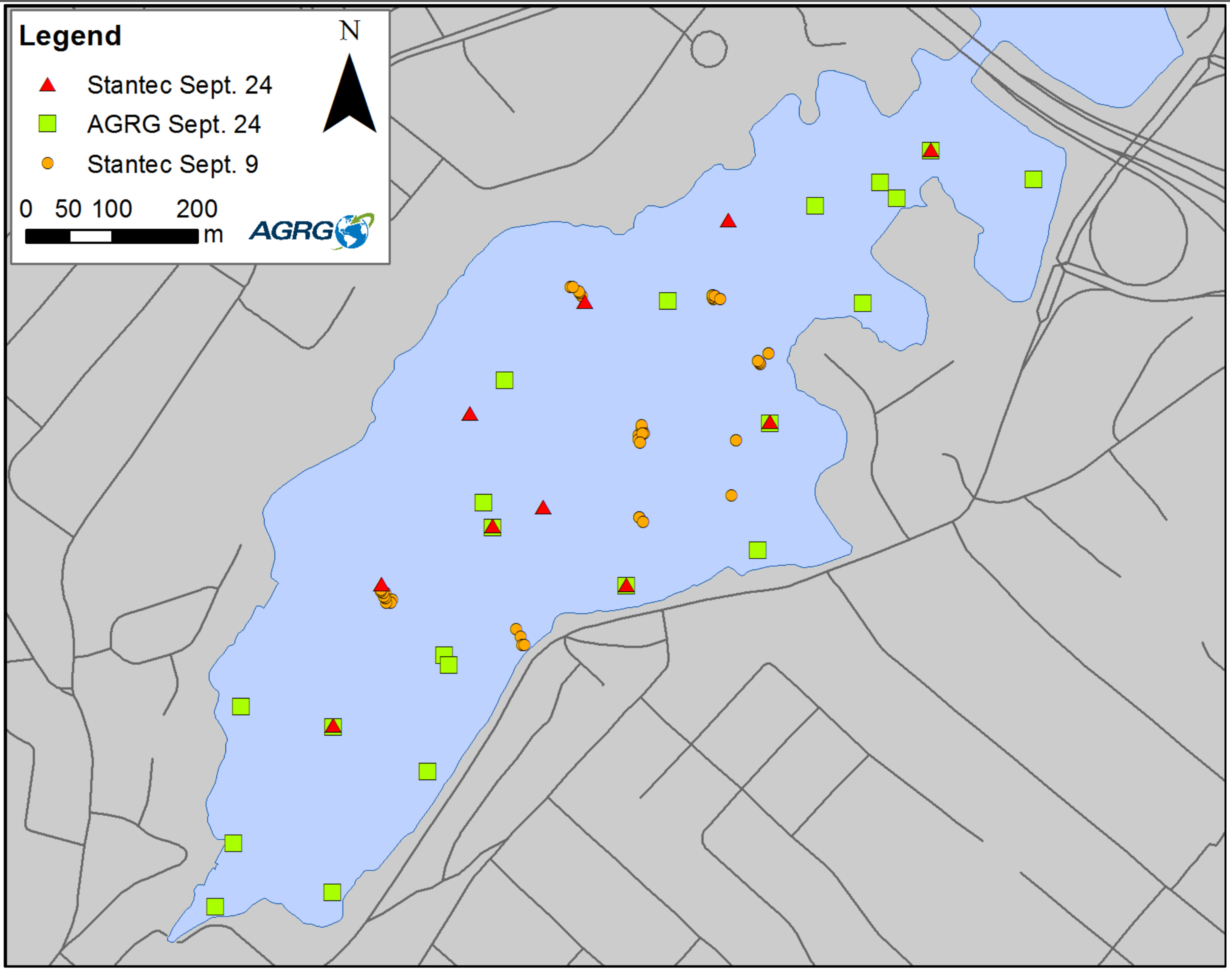

Figure 2.7: Ground truth data coverage obtained by AGRG and Stantec on various dates in September 2014.

Secchi depths were obtained on September 24 and ranged from 0.8 m to 4.2 m, where depths less than 3.0 m did not disappear but hit the bottom, and average turbidity ranged from 0.79 NTU to 1.4 NTU, although 27/28 measurements were between 0.79 and 0.98 NTU (Figure 2.8). Highest turbidity was found in the center of the lake, with higher values at mid-depth and near-bottom than at the surface; near the shore, surface turbidity tended to be higher than mid-depth and near-bottom observations. However, it should be noted that all values were very low: a value of 1 NTU would be considered a safe level for human consumption in many places (World Health Organization). In general, higher turbidity values correlated with shallower Secchi depths.

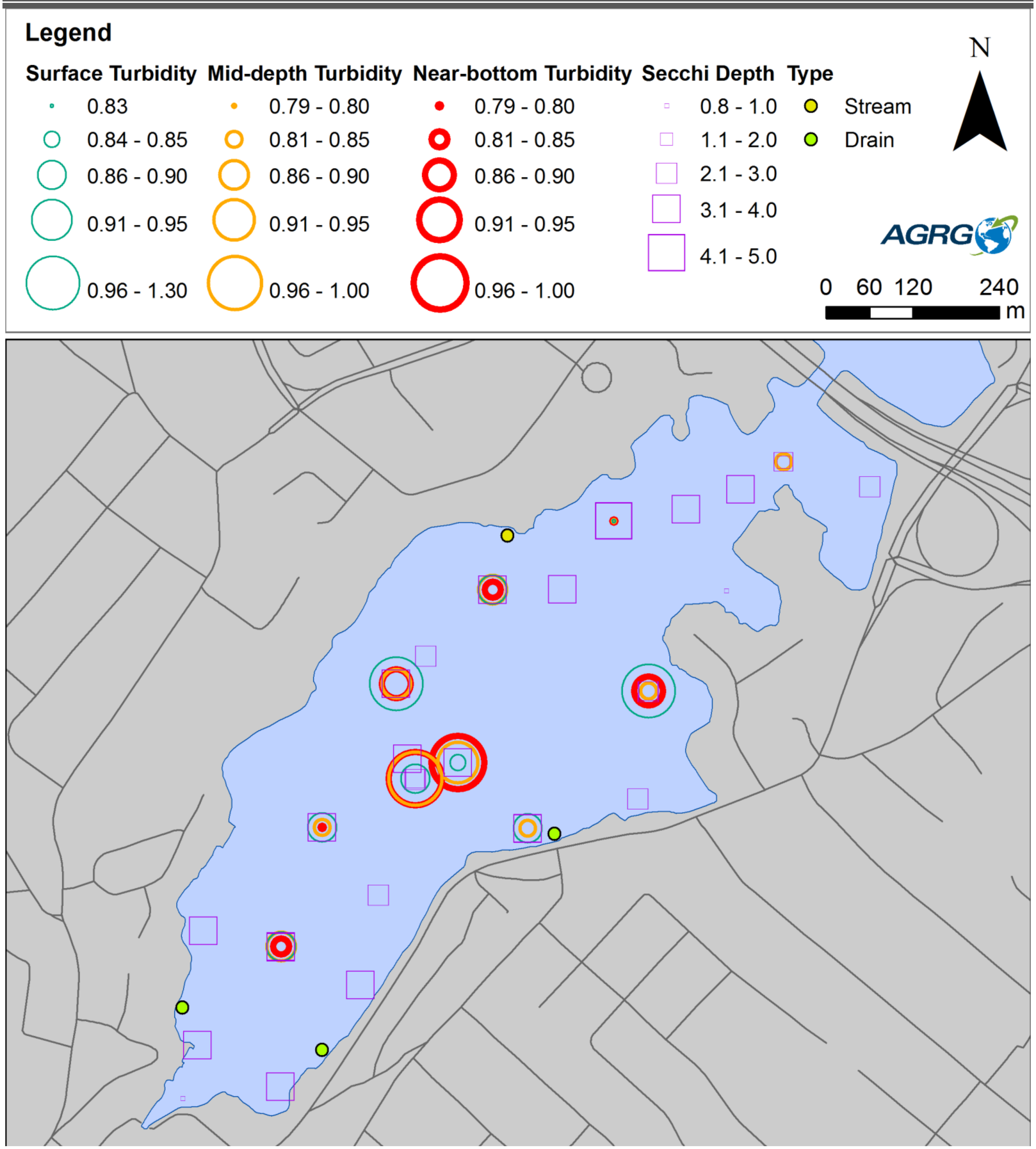

Figure 2.8: Turbidity data and Secchi depth measurements taken on Sept. 24. The correlation between deeper Secchi depth (shallower) and lower turbidity (higher) is evident.

2.5 Aerial Survey Data Processing

2.5.1 Lidar Processing

Processing of lidar products was achieved using a standardized approach wherein immediately after collection, data was downloaded and initial quality control processing was done to assess the GPS and inertial measurement unit (IMU) performance, the blended solution of these, the depth penetration of the bathymetric laser in the water column, and the overall study area coverage. Once initial quality checks were passed, lidar aircraft flight trajectories were refined and blended GPS/IMU positions were computed more thoroughly to establish the best solution possible for laser shot and photograph locations and orientations. GPS/IMU processing was performed using NovaTel Inc. Inertial Explorer.

Raw lidar pulse backscatter information was interpreted into discrete point information (LAS format) using Leica-AHAB Lidar Survey Suite (LSS) software which accompanies the Chiroptera II platform. Initial point classifications and various metrics critical to laser based bathymetric depth calculations such as water refraction and water surface elevations were computed and adjusted in LSS as well. Resulting point classifications were then further refined using the TerraScan extension to Microstation by TerraSolid. This refinement process included, for example, the more diligent differentiation of water surface return points from shallow bathymetry and low vegetation from ground. Special attention was paid here to differentiating submerged aquatic vegetation (SAV) return candidate points from valid bathymetry, water surface returns, and noise. All points were further classified into overlapping and non-overlapping points in overlapping areas based on their proximity to the nadir (the point directly below the aircraft).

Once classified thoroughly, standard lidar and bathymetric lidar raster products were constructed in ArcGIS and Python. Such standard raster datasets include a Digital Elevation Model (DEM, Figure 2.9a) wherein only valid ground elevations are represented (vegetation, buildings, etc. are removed) and a Digital Surface Model (DSM, Figure 2.9b) containing all valid returns (ground, vegetation, buildings, etc.). All elevation raster data products were constructed in 32 bit floating point precision, with a ground spatial resolution of 1x1 meter, are projected in the North American Datum 1983 (NAD 83) Universal Transverse Mercator (UTM) zone 20 North, and referenced vertically to the Canadian Geodetic Vertical Datum of 1928 (CGVD28). Lidar bathymetry data are rasterised both as bathymetric elevations (adherent to the spatial description as described above), as well as depth values relative to the water surface observed by the laser system during time of flight.

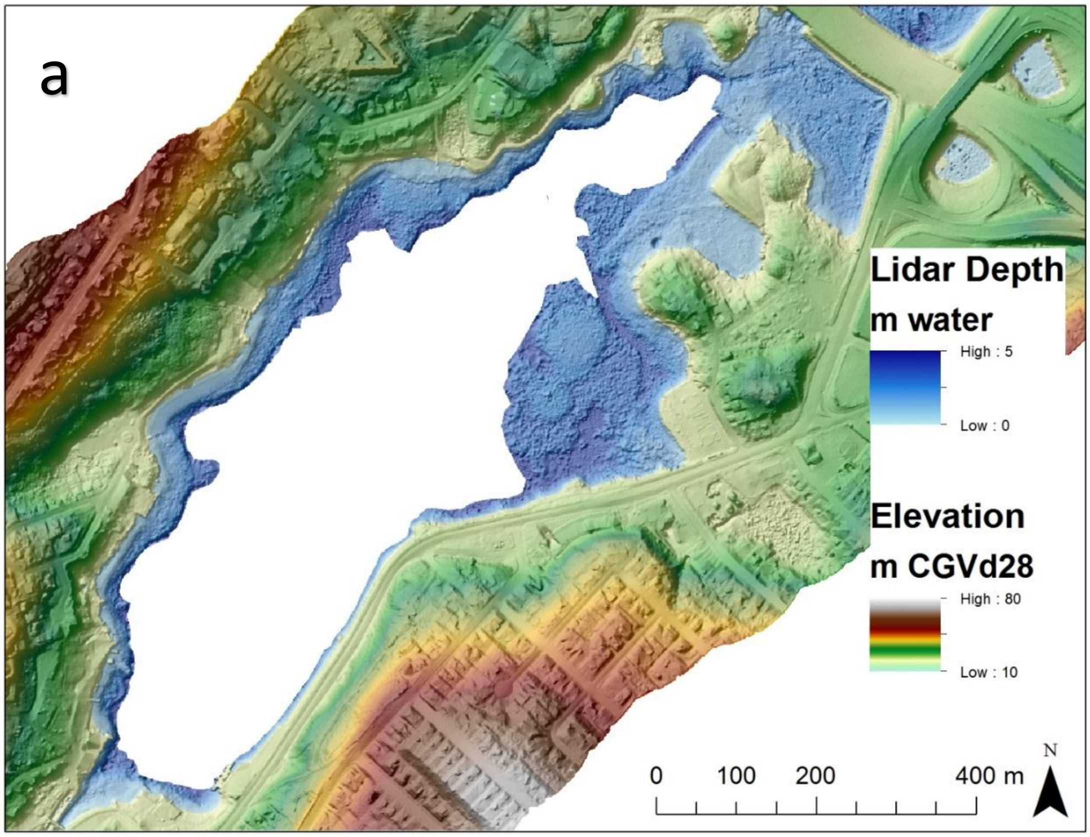

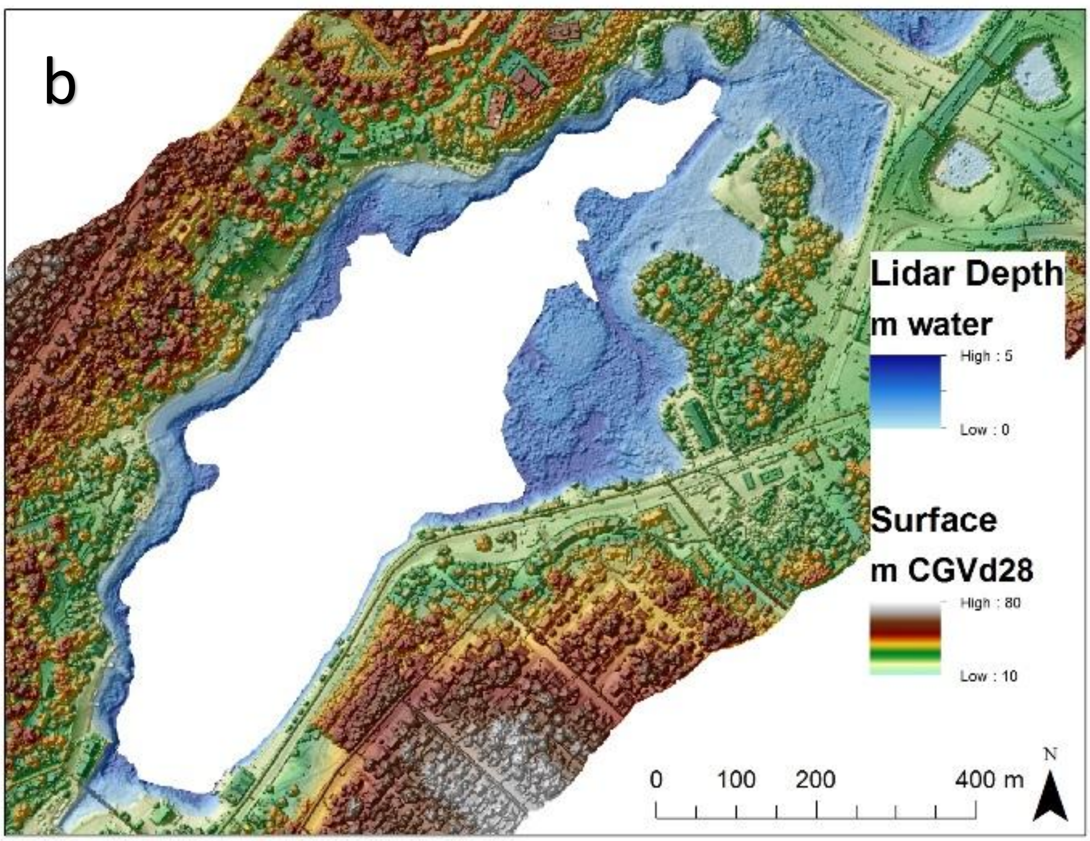

Figure 2.9: (a) Digital Elevation Model (DEM) and (b) Digital Surface Model (DSM). Both colorized by height and enhanced with surface relief models, and both are overlain by laser-based bathymetry (coloured in blue).

2.5.2 Lidar Reflectance

Lidar reflectance illustrates the variance of lidar return amplitudes across various ground features (Figure 2.10). Lake features are captured and represented from the green bathymetric laser return amplitudes (inside the water extent, red line on Figure 2.10) while the ground features are captured and represented by the NIR topographic laser (outside the water extent). Returns from the green bathymetric laser exist over ground but are a coarser ground spacing than the NIR laser (10:1) and are typically exposed to the maximum sensitivity of the sensor. Reflectance raster products were constructed with the same spatial characteristics as described above.

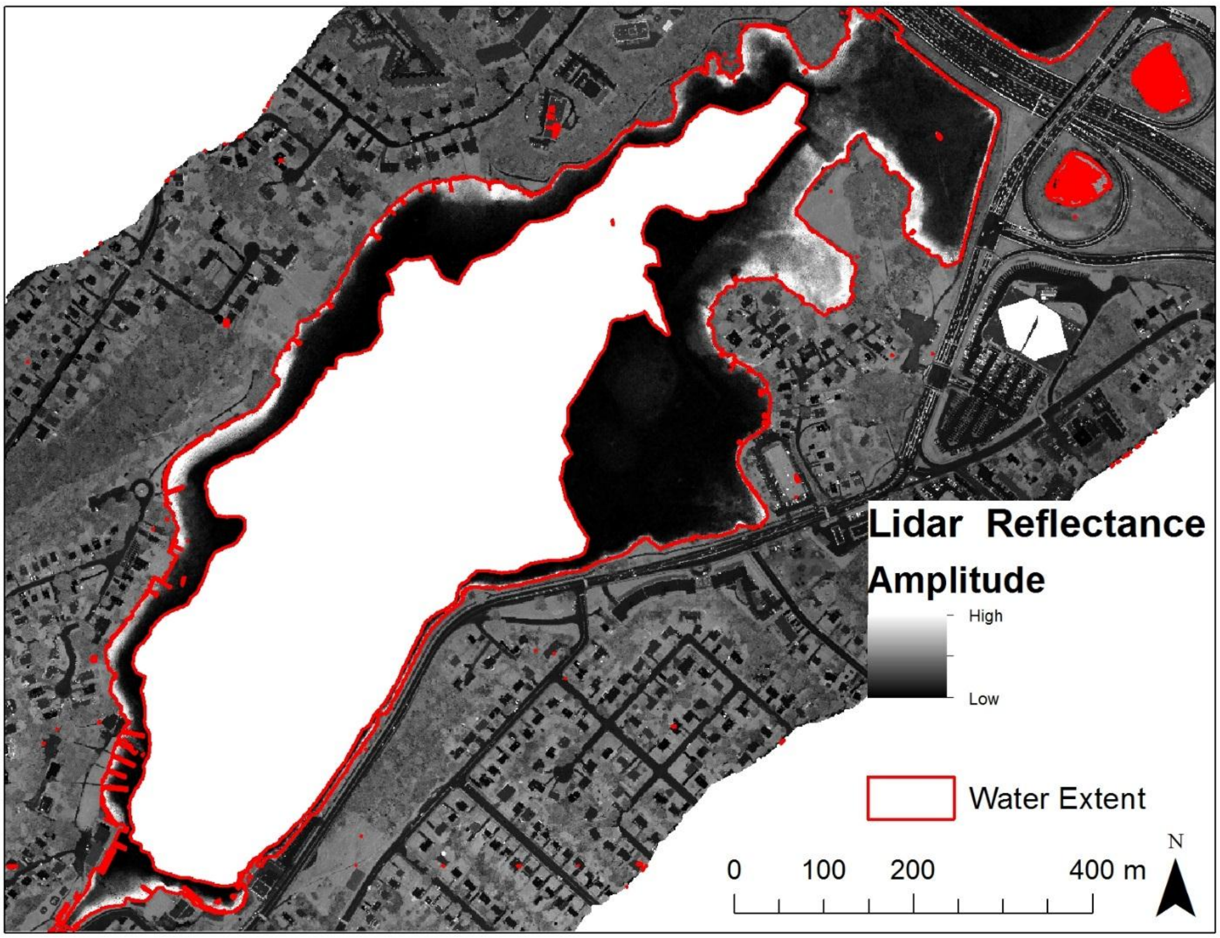

Figure 2.10: Lidar reflectance of the lakebed (inside the red line) and the ground (outside the red line) illustrating the variance of lidar return amplitudes across various ground features.

2.6 Air Photos

Aerial photographs were collected through the Chiroptera II system simultaneously with bathymetric and topographic lidar data using the onboard Leica RCD30 camera system that collects high resolution images across three bands of visible light (RGB) as well as a NIR band. Image frame exposures were not modified during the time of flight to enable simpler image mosaicking. Image frames were digitally exposed with a 16 bit pixel depth to ensure a high amount of signal information was available in the dark-coloured submerged portion of the images.

Aerial photographs were directly georeferenced to the ground using exterior orientation data from the processed flight trajectory information which was gathered across all image frames. Georeferenced images were individually orthorectified into parallax-free rasters by removing relief displacement from the images using the DSM constructed from the co-synchronous topographic lidar data. Where required, colour balancing was applied before mosaicking to ensure continuity between individual frames. The final mosaic of the study area was constructed at a ground cell spacing of 5 cm and contains RGB and NIR reflectance bands (Figure 2.11).

Figure 2.11: Processed true color aerial photograph mosaic captured simultaneously during the topo-bathymetric lidar survey.

2.7 Submerged Aquatic Vegetation Mapping

2.7.1 Presence/Absence

An SAV presence/absence mapping methodology was developed which incorporates pertinent information collected using the Chiroptera II platform including: (1) a high resolution 16 bit digital aerial photograph mosaic as collected by the onboard camera system, (2) the Lake Banook water surface at time of flight collected with the onboard topographic laser system, (3) lake bathymetry and submerged non-bathymetry points, where available, as collected by the onboard bathymetric laser system, and (4) ground truth SAV presence/absence information.

Presence/Absence of submerged aquatic vegetation was determined using a radiometric analysis of recorded reflectance values across various image bands and the bathymetric laser channel (532 nm). These data were first normalized across depth using a novel approach developed at AGRG based on reflectance. Depth information for the lake was constructed in a raster format by subtracting the lidar derived lake bathymetry model from a model of the surface of the water captured during the flight by the topographic laser system; both of these models were elevation grids referenced to CGVD28. The process of depth normalization was based on the principle that any feature, e.g., a sandy bottom or a pebbled bank, should have a similar reflectance measurement across all depths. A relationship between depth and changes in reflectance values was empirically derived for each individual band of the aerial photography as well as the backscatter amplitude values collected by the bathymetric laser. Two separate depth normalization routines were performed where: (1) darker bottom features are used to develop the empirical relationship (Method 1, Figure 2.12); and (2) lighter features are used (Method 2, Figure 2.13).

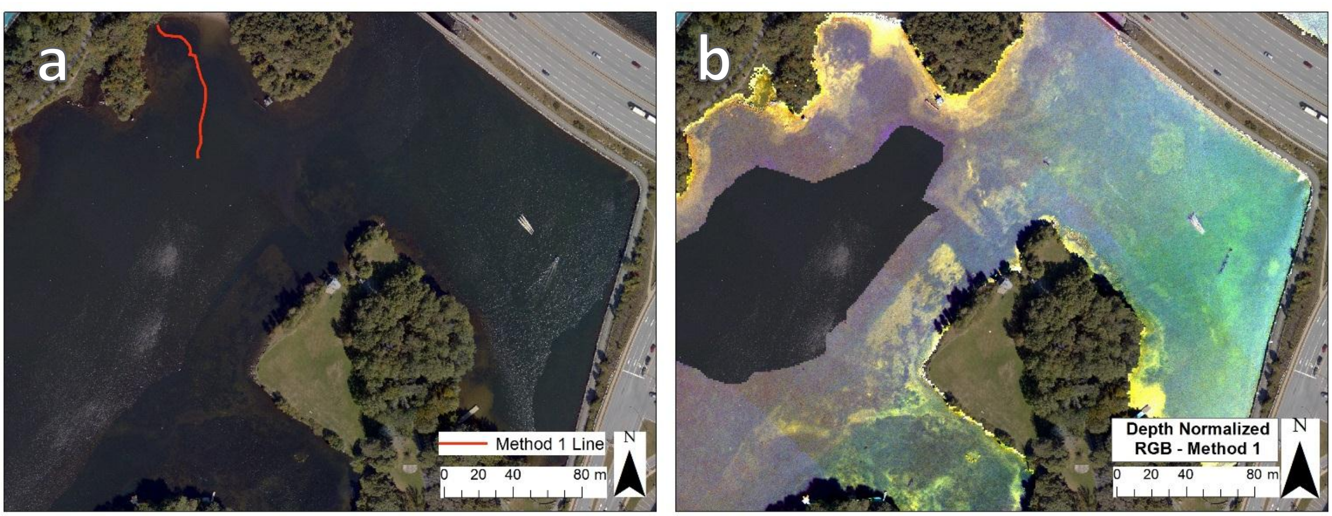

Figure 2.12: Method 1 depth normalization of photo reflectance is conducted by normalizing reflectance using similar dark features (a becomes b). The red line represents user-selected feature of similar bottom reflectance.

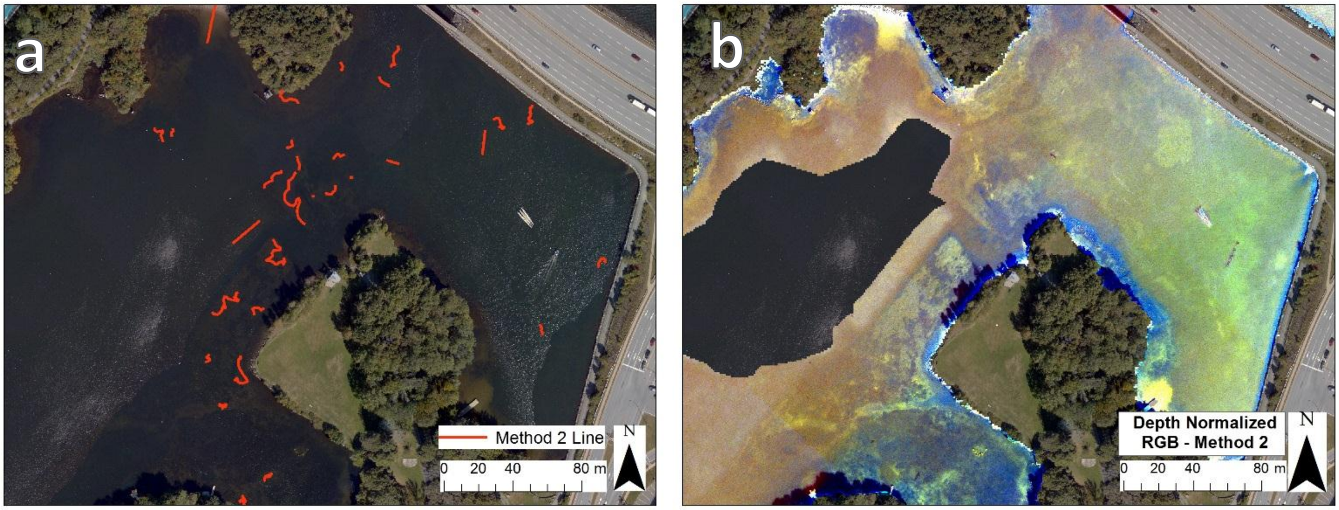

Figure 2.13: Method 2 depth normalization of photo reflectance is conducted by normalizing reflectance using similar light features (a becomes b). The red lines represent user-selected features of similar bottom reflectance.

Once depth normalized, each individual band of the aerial photographs and the bathymetric channel laser data are assessed visually and assigned a threshold value that best represents the break point between presence and absence of SAV; the breakpoint is simple to define once the light attenuation effect of water at depth is accounted for and SAV appears in high contrast to dark sediments (Table 2). It is of note that the blue and NIR image bands as well as the topographic laser reflectance values were observed to be much less effective at differentiating bottom features because those wavelengths interact more strongly with the water column itself. The threshold analysis was therefore conducted on the remaining bands using both employed depth normalization methods resulting in a total of six presence/absence datasets of varying effectiveness (Figure 2.14 and Figure 2.15).

Table 2: Two depth normalization methods were employed over three radiometric raster bands for a total of six bands used to identify SAV. Each radiometric raster band is weighted based on the assessed effectiveness wherein higher values are of greater effectiveness.

Depth Normalization	Band	Threshold	Weighting
Method 1	Red	15035	50
	Green	16995	10
	Bathymetric Laser	49000	25
Method 2	Red	61000	10
	Green	34100	10
	Bathymetric Laser	58000	10

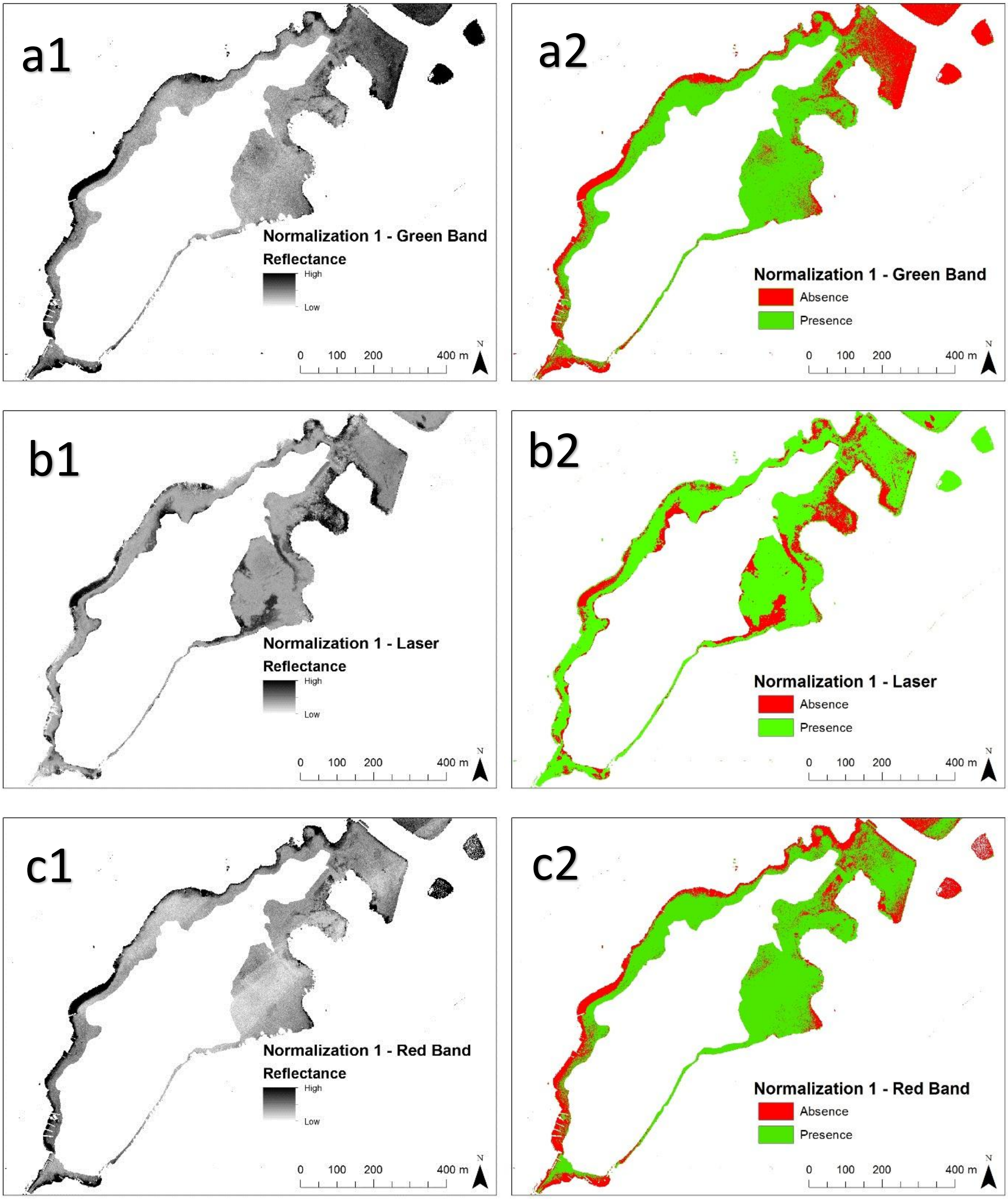

Figure 2.14: Method 1 depth normalized raw greyscale radiometric raster bands (a1, b1, c1) and threshold binary presence/absence submerged aquatic vegetation layer (a2, b2, c2) produced from each band. Method 1 uses the reflectance of a continuous dark feature.

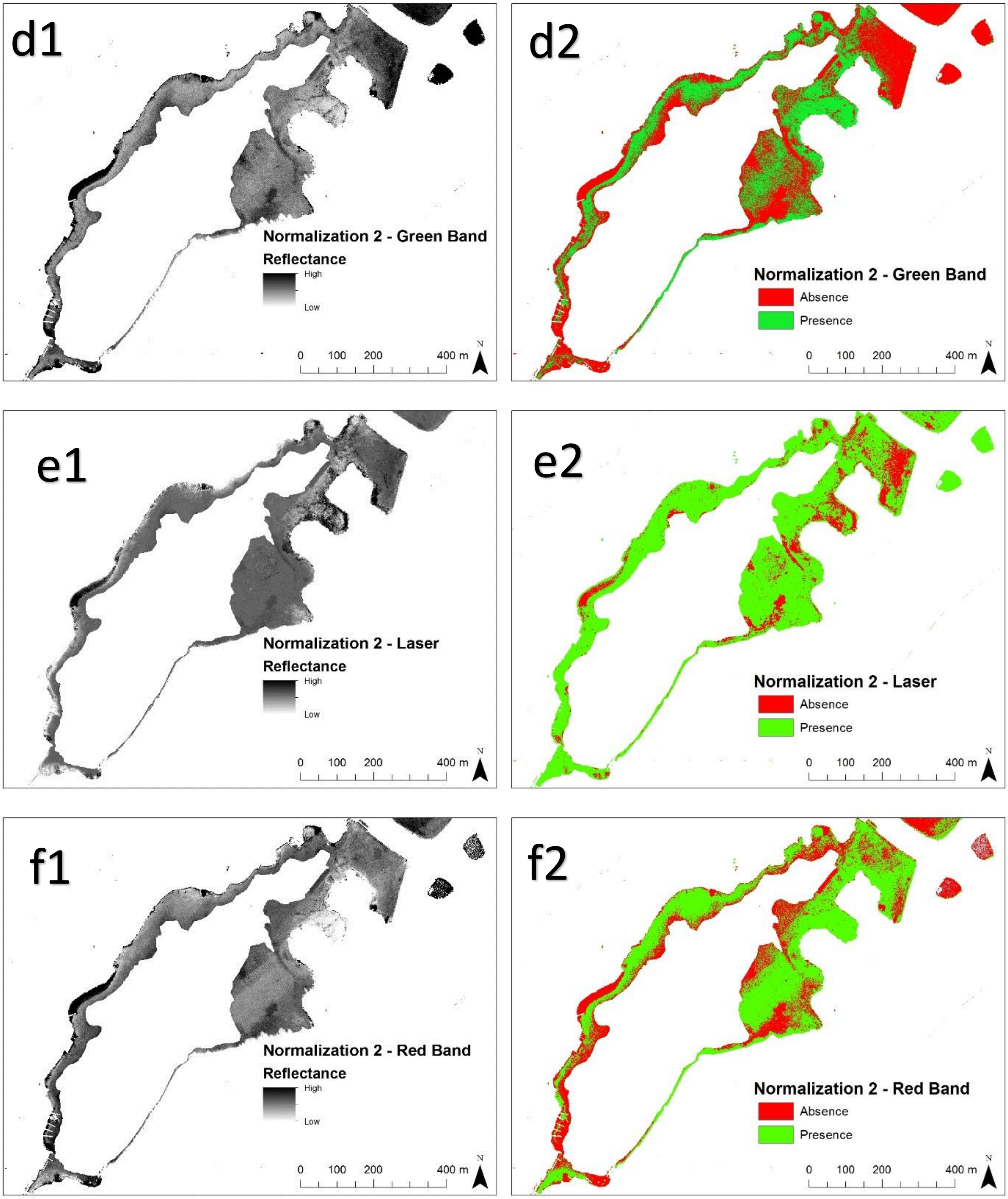

Figure 2.15: Method 2 depth normalized raw greyscale radiometric raster bands (a1, b1, c1) and threshold binary presence/absence submerged aquatic vegetation layer (a2, b2, c2) produced from each band. Method 2 uses the reflectance of a continuous light feature.

A presence/absence map of SAV was constructed by accumulating each of the six SAV presence/absence raster datasets derived from individual bands into a single dataset (Figure 2.16a). The contribution of each of the bands was weighted based on their overall effectiveness and assessed visually to better represent the SAV distribution as observed (Figure 2.16b, Table 2). The resultant weighted SAV presence/absence dataset was then simplified interactively again using a threshold method to depict a final binary state of SAV presence and absence which is presented in the Results section. Success in this method was determined when the resultant SAV distribution was best adherent to a visual comparison with the aerial photographs.

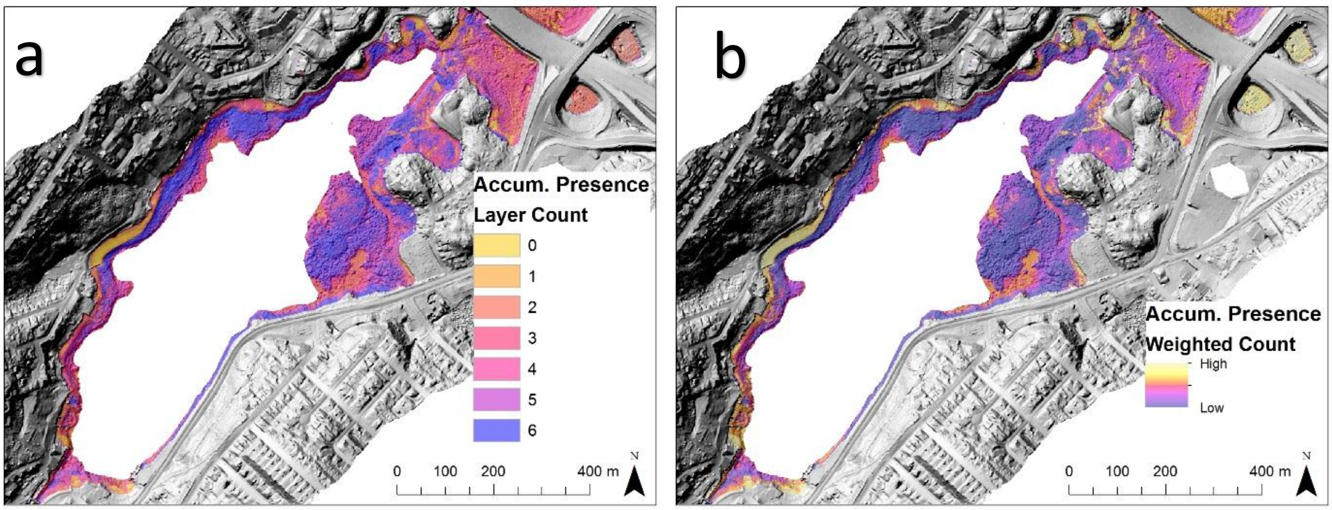

Figure 2.16: (a) Accumulated presence/absence of each of the six radiometric raster bands; and (b) similarly when weighted appropriately based on apparent effectiveness when compared visually to air photo.

2.7.2 Height and Roughness

Using the point data of the submerged bathymetric laser returns, specific processing was conducted to differentiate valid bathymetric points from: (1) noise, (2) water surface returns, and (3) valid non-bathymetric points. Using the valid non-bathymetric points as an analogous metric for SAV presence in the water column, localized SAV heights were estimated where presence was also identified in the radiometric presence/absence analysis. These heights are estimated relative to the nearby valid bathymetric points and are thus represented in meters from bottom. This analysis was conducted on a 1x1 meter grid and exhibits data gaps where no SAV above the bottom are detected at that resolution.

An analysis of the bottom roughness of the lidar bathymetry was performed where SAV presence was determined. This was computed using the deviations of bathymetry slope and slope aspect. The bathymetric lidar data is rasterized at a cell resolution of 1x1 meter, whereas the neighborhood analysis of lidar roughness results in much coarser dataset (~3x3 meter) though no data gaps would exist.

Height and roughness maps are presented in the Results section.

3 Results

3.1 Lidar Depth Validation

Lidar derived depths validated very well relative to interpolated high resolution multibeam beam survey data provided by GSC (King and Geological Survey of Canada, 2008). When comparing the lidar bathymetry (Figure 3.1a) to acoustic multibeam bathymetry (Figure 3.1b) as a set of 1x1 meter spatial resolution floating point depth rasters, a mean difference of -0.024 m was observed, indicating that the lidar was on average 2.4 cm deeper than the multibeam data. The analysis also showed a standard deviation of 0.382 m (38.3 cm). Not only does this indicate the two datasets show vertical agreement within the vertical speculations of the bathymetric lidar, but also that the water elevation during the time of both surveys was very similar. The spatial distribution of the difference of these two datasets does not indicate any systematic lateral offset, suggesting there are no georeferencing or grid transformation discrepancies (Figure 3.2). It is notable, however, that the lidar data does appear to have more vertical difference than the multibeam data in areas of greater texture, which is in agreement with the higher detail observed in the lidar data when compared to the interpolated multibeam survey (Figure 3.2). The linear artifacts of the multibeam data are also evident in Figure 3.2.

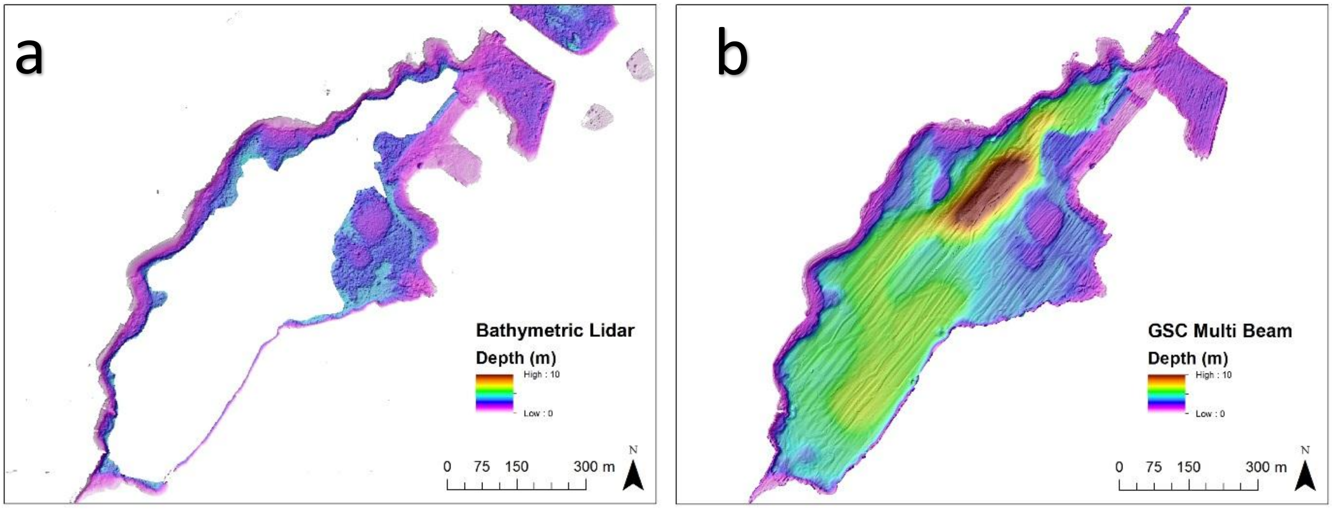

Figure 3.1: (a) Lidar bathymetry of Lake Banook coloured by depth and shaded by surface relief; (b) interpolated-continuous multibeam GSC survey data, similarly coloured.

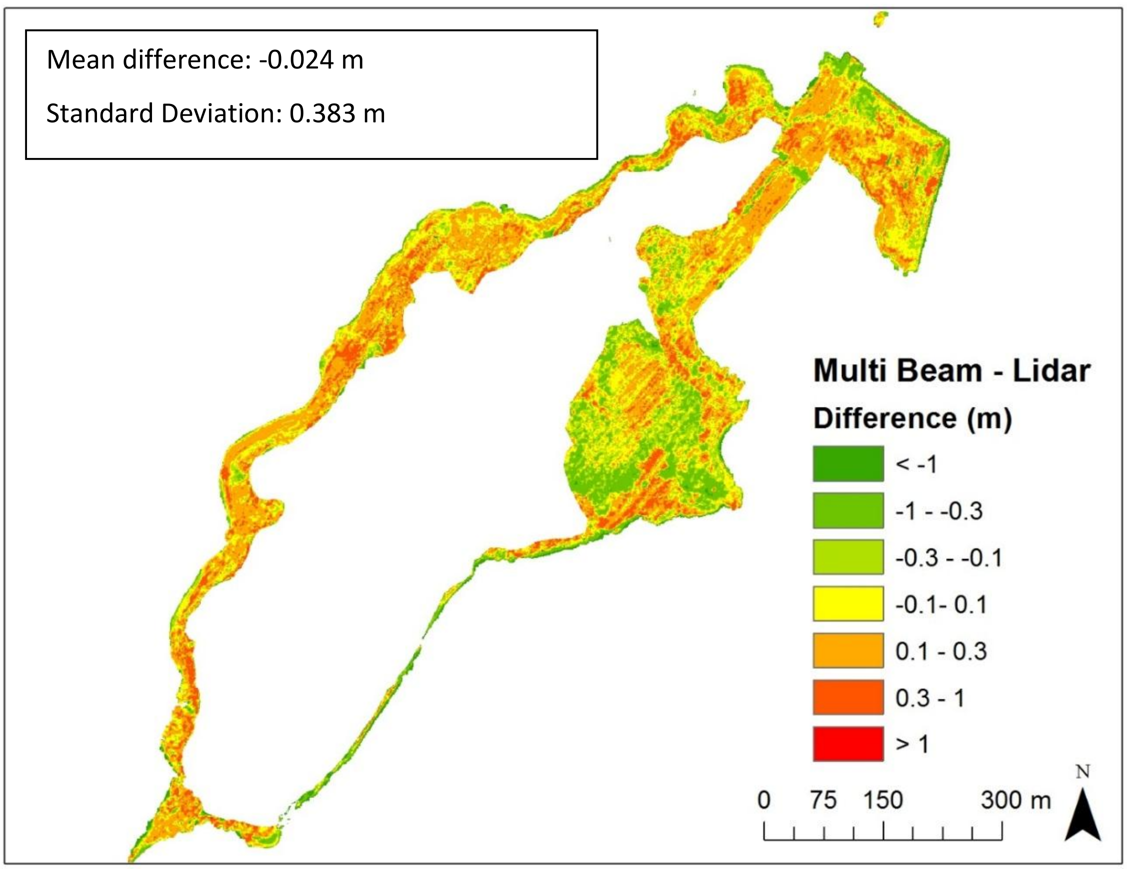

Figure 3.2: The lidar is validated with a difference analysis against the multibeam sonar survey provided by the GSC. The analysis indicates the lidar is within an average of 2.4 cm depth of the sonar survey with a standard deviation of 38.3 cm. Note that the discrepancy in depths mimics the greater textural detail captured by the lidar survey and highlights the linear artifacts of the multibeam data.

3.2 Submerged Aquatic Vegetation

3.2.1 Presence/Absence

The final presence/absence binary map derived from the radiometric raster band analysis is considered to be the final result of this study (Figure 3.3). This map product has a 20x20 cm ground resolution as it is derived principally from depth normalized air photos. The SAV presence/absence map agrees well with air photos. In deeper areas, which are not well captured by the air photos, the inclusion of lidar backscatter amplitude has enabled a better differentiation of SAV and brighter reflecting bottom types such as sands. However, the inclusion of the lidar backscatter raster in some areas < 1 m depth has negatively affected the SAV map, likely because the higher pixel size of the backscatter raster (1x1 m) degrades the SAV map compared to the aerial imagery. Additionally, some features reflect strongly enough in the shallow water environment to exceed the maximum sensitivity of the laser sensor and result in gaps in backscatter amplitude data. Note that currently, false positives do exist in the presence/absence map in areas of tree shadows.

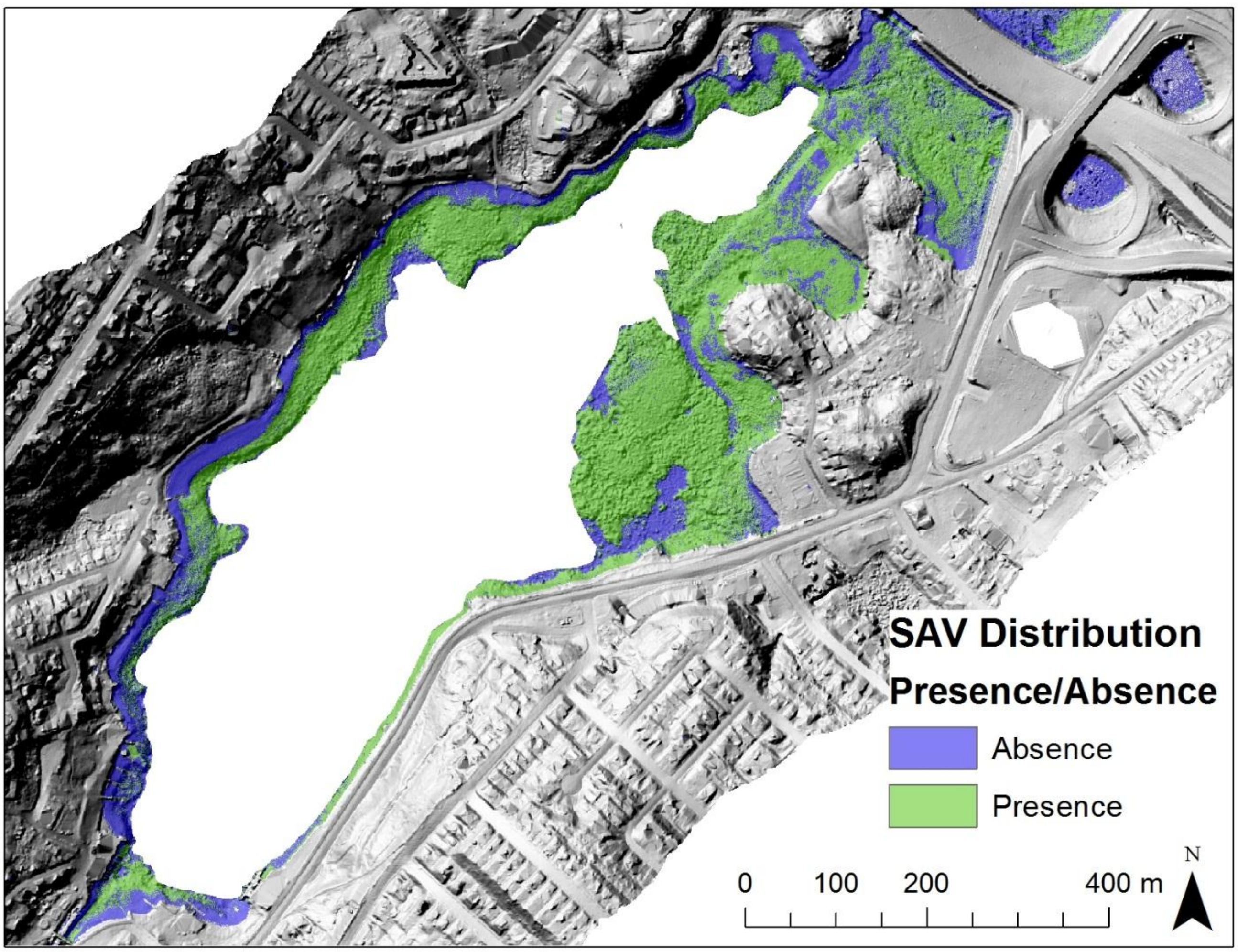

Figure 3.3: The final submerged aquatic vegitation (SAV) map as collected by the Chiroptera II topo-bathymetric lidar sensor for Lake Banook in September 2014. Green color indicates the detection of vegetation and blue indicates areas of little or no vegetation. The image has a backdrop relief model of ground information collected by the topohraphic laser during the survey.

3.2.2 Height and Roughness

In addition to a direct presence/absence analysis, we have conducted an analysis of two additional lidar-derived features which are considered relevant to SAV characteristics and can perhaps can assist further analysis for further refinement of the SAV presence/absence map, for differentiating SAV types, and perhaps SAV biomass/volumetric analysis. SAV roughness (Figure 3.4) appears to be characteristic of shallow water SAV on the eastern shores of the lake. This may perhaps indicate a discrepancy in conditions throughout the lake that allow for SAV of different types or growth patterns to manifest spatially. It is also possible that this trend correlates to a higher artificial infilling of coarse rock on the eastern side of the lake, whereas sand infilling is more common on the west side of the lake for swimming areas. Specific validation of this analysis has not been performed with ground truth. This analysis could be useful to better assess the SAV presence/absence detection with regard to dark and coarse bottom features such as dark bioturbated soils atop coarse boulders which appears to be noted frequently in the ground truth data.

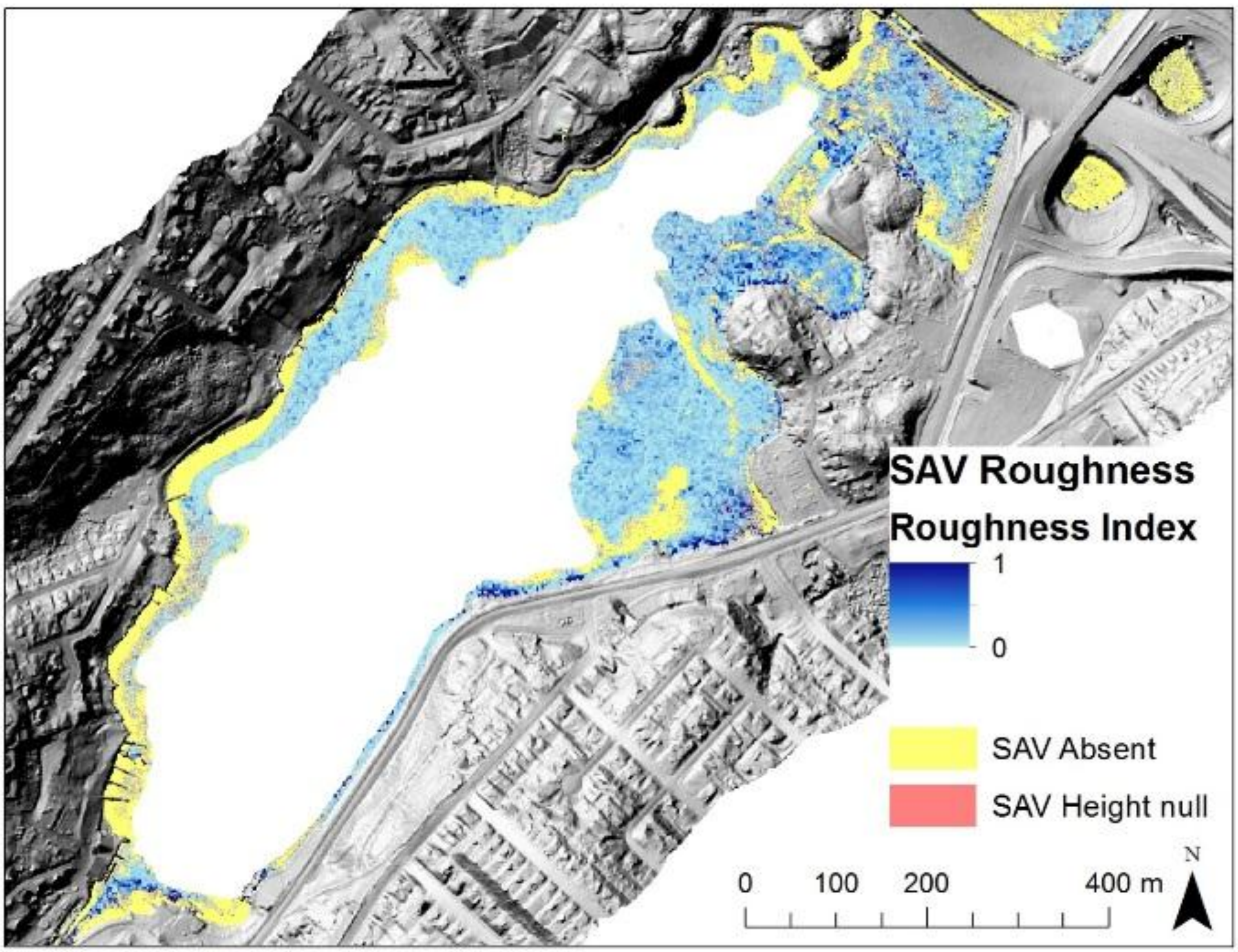

Figure 3.4: Bottom roughness where SAV presence has been detected may be a good indicator of SAV type or density. This figure indicates the SAV roughness as a index where 1 is high roughness and 0 is low roughness. Yellow indicates areas where SAV was determined to be absent in the radiometric analysis.

SAV heights from the bottom could further be used to distinguish SAV types and grounding characteristics. SAV height is determined from classified submerged lidar points and their relative height from nearby bottom points (Figure 3.5, blue areas). Areas where radiometric analysis indicated no SAV presence are classified as SAV absent (Figure 3.5, yellow areas), and areas where radiometric analysis determined SAV presence but no classified sumberged lidar points exist (thus no height measurements) are classified as SAV Height Null (Figure 3.5, pink areas). SAV height is presented as an absolute value in meters from bottom, rather than a range, and can thus be of great use for any volumetric estimation.

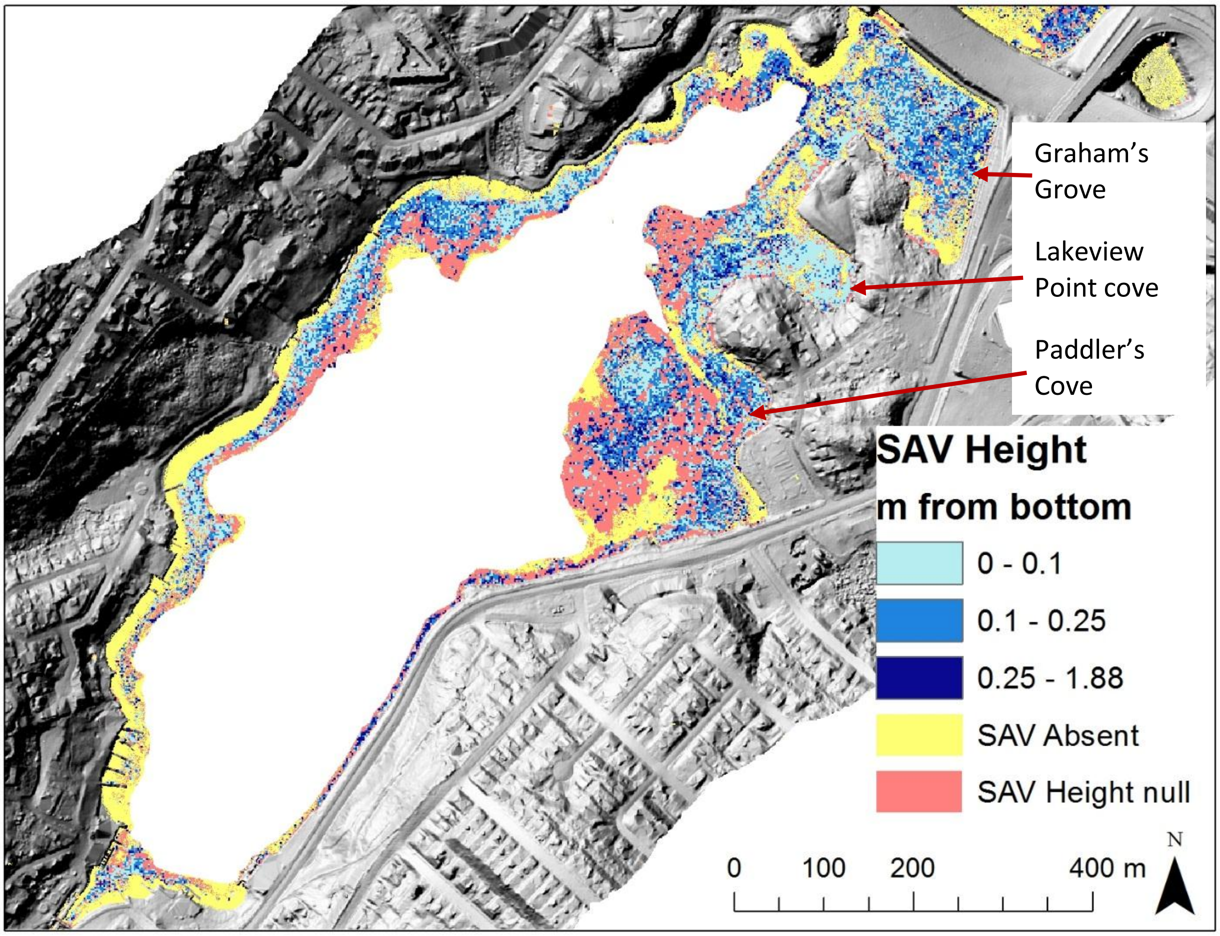

Figure 3.5: SAV height is determined from classified submerged lidar points and their relative height from nearby bottom points. Heights are thus represented as meters from the bottom (blue scale). Yellow represents areas where radiometric analysis indicated no SAV presence. Pink is where radiometric analysis determined SAV presence but no classified sumberged lidar points exist (thus no height measurements).

SAV appears to grow highest just south of the Highway 111 Bridge in Graham's Grove, and south of the sunken island off Paddler's Cove, (middle of Figure 3.5). According to height analysis, each of the three cove areas on the eastern portion of the lake exhibit different patterns of growth. Graham's Grove exhibits a consistent distribution and typically medium height SAV, the middle cove off Lakeview Point exhibits well distributed SAV with consistently the shortest height (typically <10 cm), and Paddler's Cove exhibits the highest SAV in a more sporadic grown pattern.

3.2.3 Validation and Comparison

In addition to visual comparison with the aerial photographs, the of the SAV presence/absence map was validated by comparing it to ground truth data collected by AGRG and Stantec in September 2014 (Figure 3.6). Unfortunately the majority of the ground truth data collection occurred in the deeper parts of the lake where the lidar did not penetrate, but where data exists there was excellent agreement of the SAV distribution map with the observations. The SAV map correctly detects SAV presence 83% of the time, and correctly detects SAV absence 80% of the time.

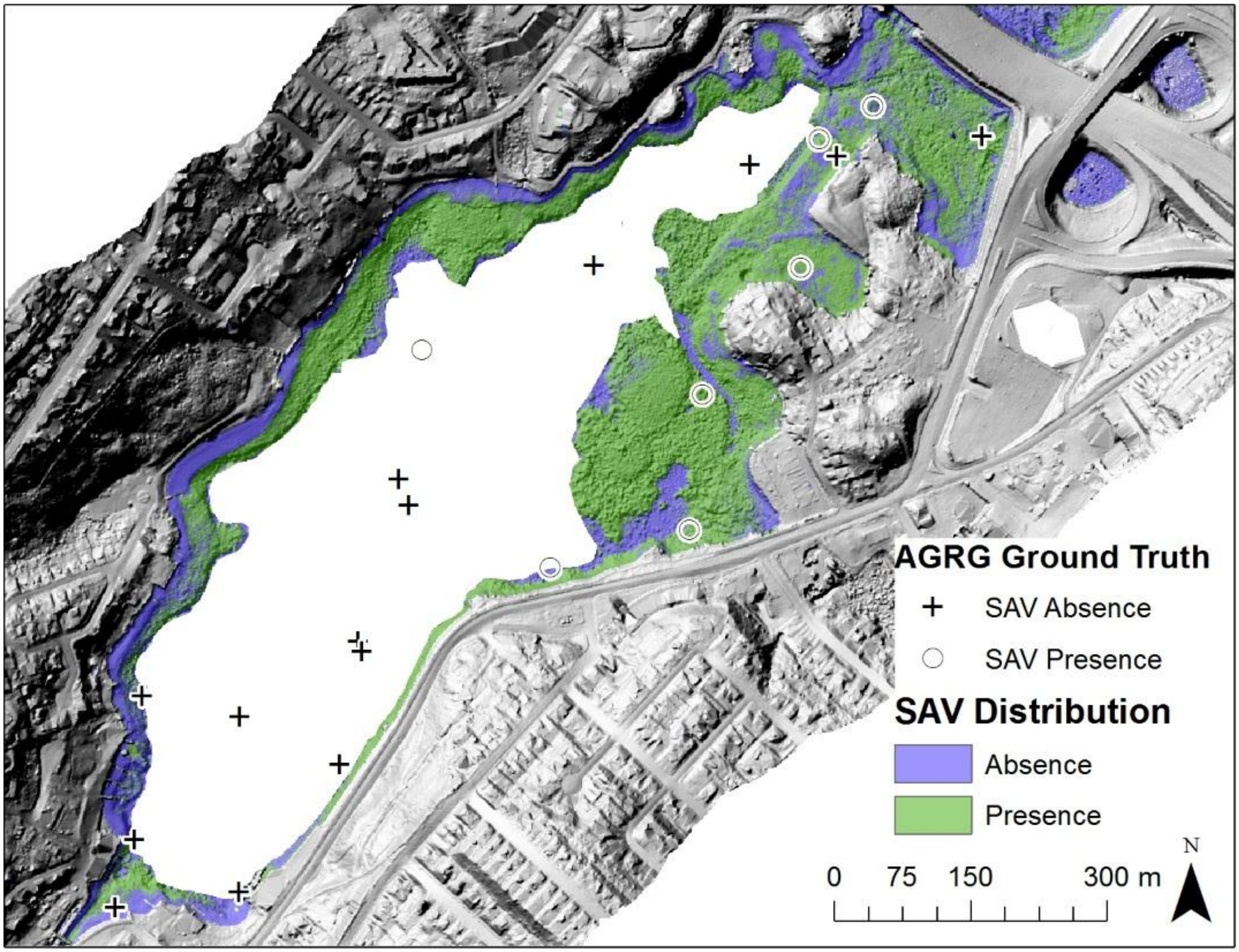

Figure 3.6: Comparison of SAV map with AGRG and Stantec ground truth observations.

We have compared ground truth and maps by Stantec (2014) of clasping-leaf pondweed (Figure 3.7a) and slender leaf pondweed (Figure 3.7b) abundance, where blue represents negligible abundance and red represents very high abundance, to our current SAV classification (Figure 3.7c). In the deepest part of the lake, no SAV was observed by any party. Unfortunately the Stantec maps have no data for Graham's Grove and Lakeview Point cove, so areas of overlap with our classification are restricted Paddler's Cove and the narrow bands of data return at the western and eastern shorelines. At Paddler's Cove we see agreement between both species of pondweed, the ground truth data, and our SAV distribution map, where all sources detected SAV. The AGRG distribution map and the ground truth points show SAV extending father south along the eastern shore from Paddler's Cove than the Stantec maps. There is general agreement of all sources along the eastern shore of the lake, and at the southern tip the Stantec maps and AGRG map detect SAV but the ground truth points do not. All along the western shore the AGRG map shows a continuous band of SAV beginning a few meters off the shore that is not identified in the Stantec maps, except for a small patch of clasping leaf pondweed north of Birch Cove Beach ("PARK BEACH"), but is consistent with ground truth presence data points.

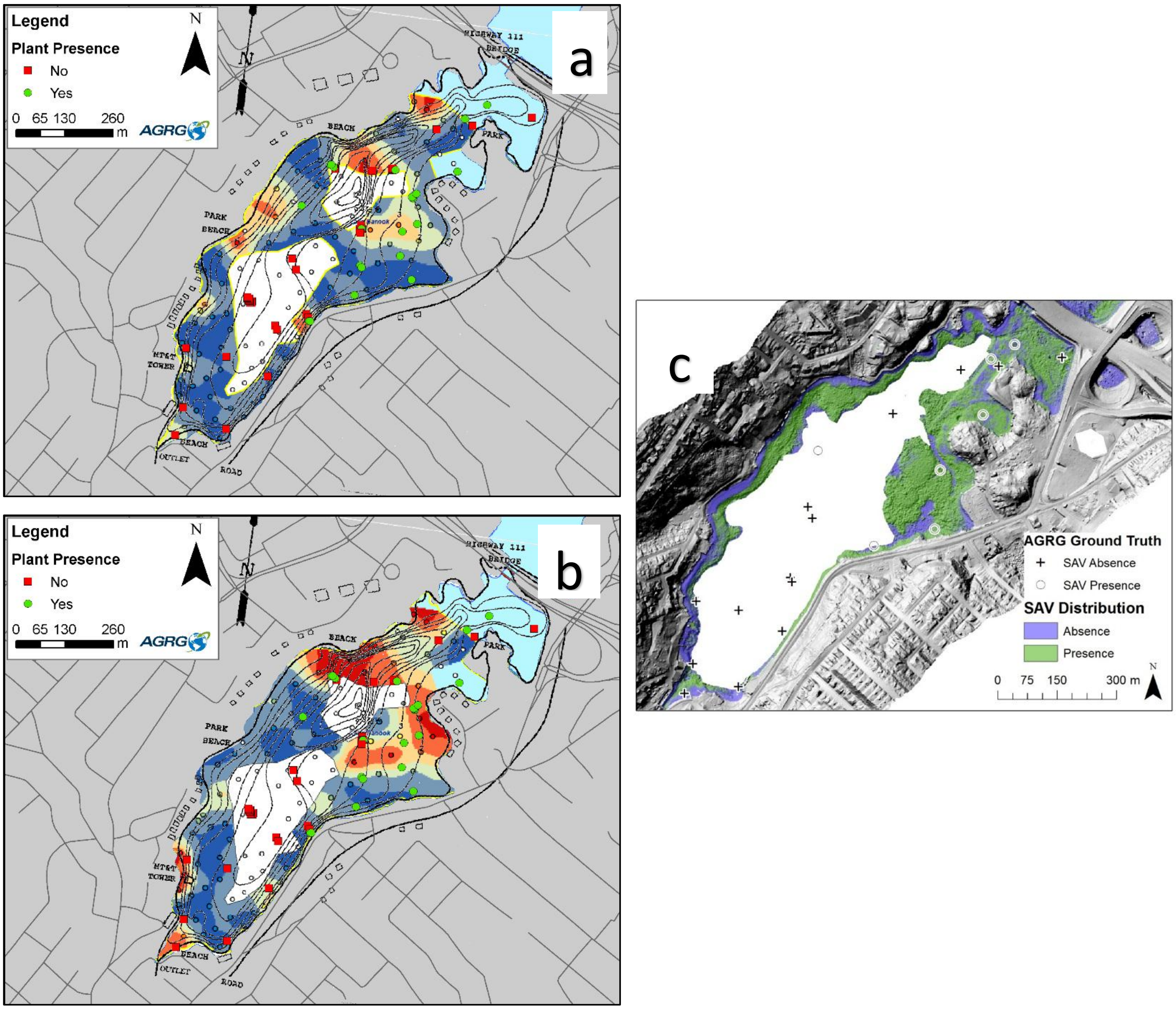

Figure 3.7: (a) Clasping leaf pondweed and (b) slender leaf pondweed abundance as classified by Stantec (2014) in November 2013, with ground truth SAV presence/absence from AGRG and Stantec in September 2014; (c) shows AGRG SAV presence/absence. Blue represents negligible abundance and red represents very high abundance

We also compared our SAV distribution and height to a set of well described underwater video camera observations provided by the GSC in collaboration with DRDC (King, 2008; Mosher, 2008). Figure 3.8 and Figure 3.9 present comparisons of the GSC observations with the orthophotos and SAV height maps for four different areas in the lake. Note that the GSC data were collected in 2007 before the lake was drained in 2008 and the SAV became a problem to boaters and swimmers, so any comparison must take that known change in SAV distribution into consideration.

In Graham's Grove and near the Highway 111 bridge we see good agreement between air photos and GSC observations (Figure 3.8a, b); agreement is especially good between SAV height and GSC observations at station 93 and 94. In Lakeview Point Cove SAV is cleary distinguishable from airphoto (Figure 3.9c) with a distribution matched in the height analysis. The descriptions of stations 71, 67, and 68 match both the air photos and the height analysis. In Paddler's Cove (Figure 3.9d) a more sporatic growth pattern is somewhat visible from airphoto. Some stations (36, 29) indicate SAV absence with mixed adherence.

In general the SAV presence/absence agrees well with the station descriptions provided by the GSC, specifically in medium depths (1 m to 2.5 m). It has been noted that some shallow areas are under-represented in the SAV distribution map, perhaps due to the inclusion of the coarser resolution lidar reflectance data or lidar reflectance saturation in shallow water, but perhaps also due to affects caused by the depth normalization process, though overall the loss of detected SAV in shallow areas is minimal (Figure 3.9c). Deeper water (>2.5 m) relies more heavily on the lidar reflectance information where air photo bottom reflectance signals are weaker. Though the lidar reflectance signal may be strong, a lack of additional good radiometric bands can hinder differentiation specifically between SAV and dark (Figure 3.9d). This can be compensated by the development of better depth normalization procedures and a process for establishing better radiometric consistency between image frames (e.g., white balance). Radiometric discrepancies are visible across the air photo mosaic and while these issues are difficult to resolve over water features, this can perhaps be alleviated with target deployment in the future. A large number of stations indicate an organic sediment (likely dark) which may presented a problem for the SAV presence/absence detection method in some areas as it relies on principally a dark radiometric response. Our current approach has some difficfulty differentiating between dark organic matter and the dark SAV itself, and we don't have the field data to tell whether the substrate has changed between 2007 and 2014 or whether we are mis-classifying it.

(a)

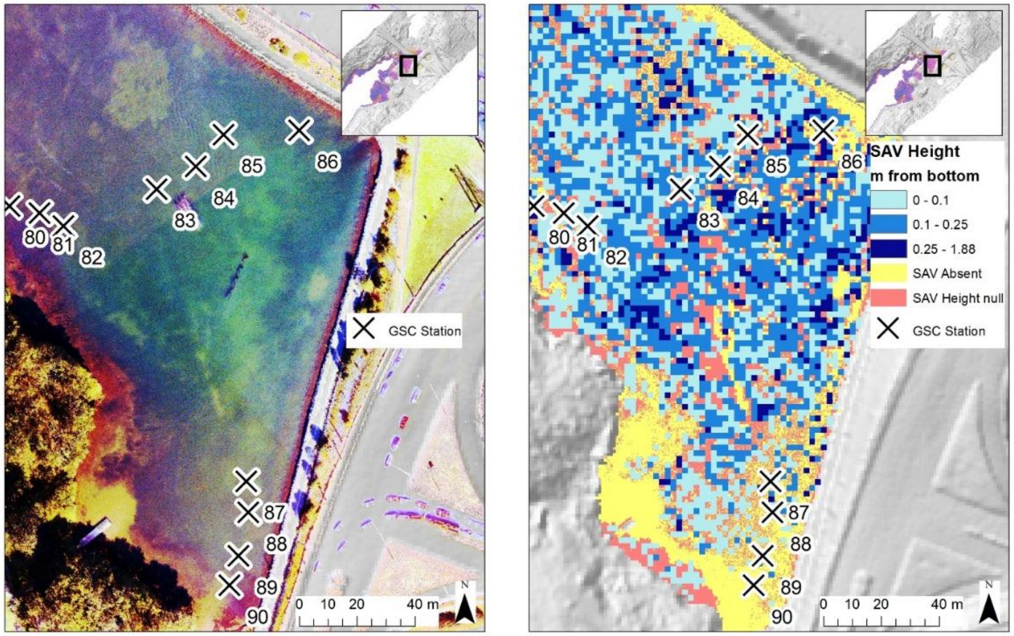

Station	SAV	GSC Description
80	1	weeds and rocks boulders soft silty sediment in between
81		boulders
82	1	highly branching weeds and boulders
83	1	weeds
84	1	weeds
85	1	thick weeds
86	1	weeds
87	1	lots of weeds
88	1	weeds
89	1	weeds
90	1	sand weed boundary

(b)

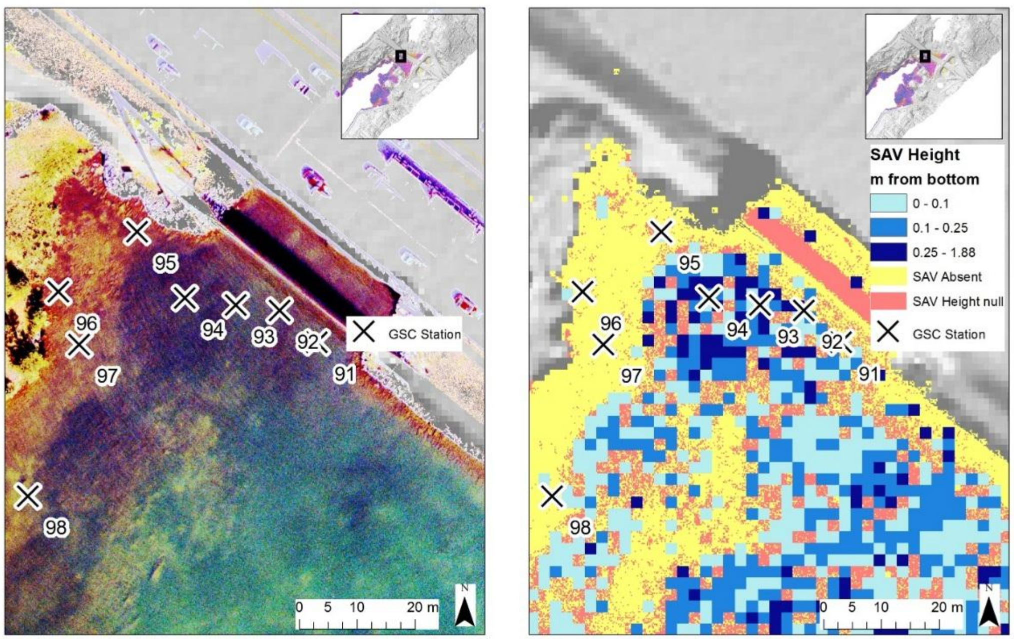

Station	SAV	GSC Description
91	1	sandy silty weedy bottom
92	1	silty bottom covered with weed
93	1	silty bottom with weeds
94	1	tall weeds
95		soft sediment boulders and cobbles
96		dust of loon silt on cobbles and pebbles
97		no boulders but some cobbles weeds on camera bottom looked silty
98		boulders and pebbles with weed

Figure 3.8: SAV in air photos, height analysis, and GSC observations at (a) Graham's Grove and (b) Highway 111 bridge. In the table, thick weeds are indicated in red, presence of SAV is marked with a 1, or a 0 if it is explicitly stated no SAV exists.

(c)

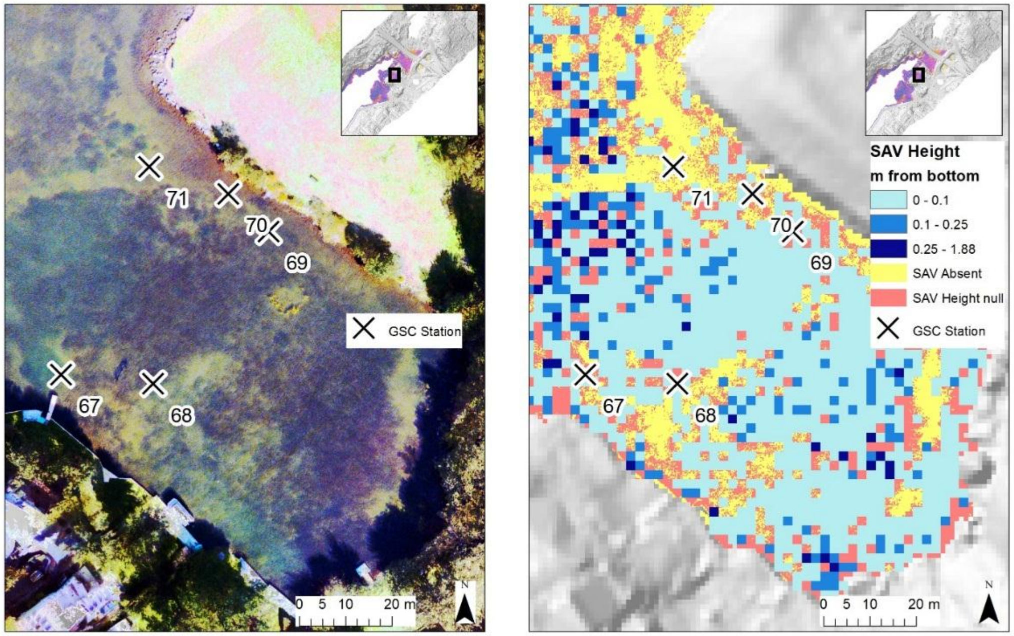

Station	SAV	GSC Description
64		boulders
67		soft weedy bottom some cobbles
68		soft weedy bottom grassy looking
69		cobbles
70		algae growth covering bottom
71		angular artificial rocks

(d)

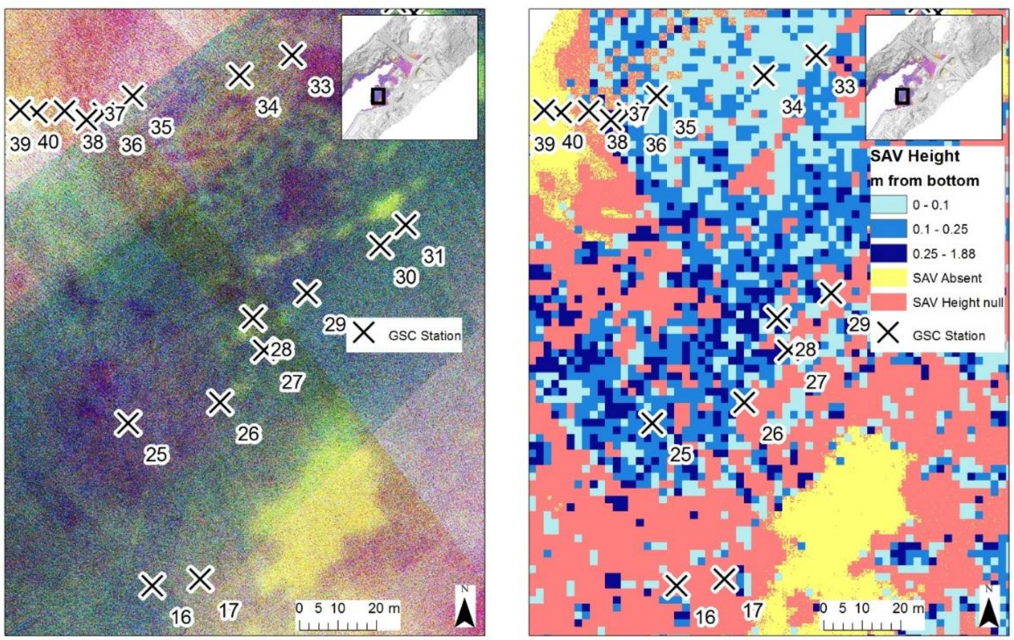

Station	SAV	GSC Description
25	1	weedy stuff; lots of weed looks like eucalyptus; thick weeds barely see bottom
26		soft silty bottom; bioturbation; worm holes; fine organics bioturbation
27	1	Mussels, bioturbation. muddy silty; some dams weeds; gossamer like weeds
28	1	mussels bioturbated soft bottom; few weeds
29	0	soft bottom no weeds or very few
33	1	no bottom due to weed
35	1	rock in weeds
36	0	boulders no weeds drop off
37		silty bottom With lots of boulders clams
39		boulders on silty bottom
40		bottom With no boulders; bioturbated soft bottom
30	1	very high bioturbation ; clams and few weeds

Figure 3.9: SAV in air photos, height analysis, and GSC observations at (c) Lakeview Point cove and (d) Paddler's Cove. In the table, thick weeds are indicated in red, presence of SAV is marked with a 1, or a 0 if it is explicitly stated no SAV exists.

3.2.4 Depth Analysis

We conducted an analysis of how SAV was distributed over depth by first dividing the bathymetric grid into 10 cm contours and calculating the bathymetric area contained within each contour. This showed that there was a large area of the DEM that fell into the contours between 1.5 m and 2.5 m and that the DEM showed very little area between 4.0 and 4.5 m (Figure 3.10, blue line). Next we calculated how much SAV was present in each depth contour using the SV presence/absence grid. This analysis showed SAV area increasing with depth up to 3.0 m, with peaks at 0.5 m, 2.25 m, and around 3.0 m depth (Figure 3.10, green line). The final step was to compute the percent of SAV coverage per depth interval to show how much of the area in each contour was composed of SAV. This showed that between the shoreline and 1.9 m percent SAV coverage stays constant at 45%, except for a sharp decrease between 0.1 and 0.4 m; it then increases steadily to a max of 85% at 3 m before sharply decreasing to 0% (Figure 3.10, red line). As noted, it is possible that dark sediments at depth were mis-classified as SAV and this is perhaps reflected in the peak of relative SAV coverage around the 3 m – 3.5 m depth mark; additionally, and the initial high value of Percent SAV coverage at 0 m may be a signature from misclassified tree shadows existing along the lakeshore.

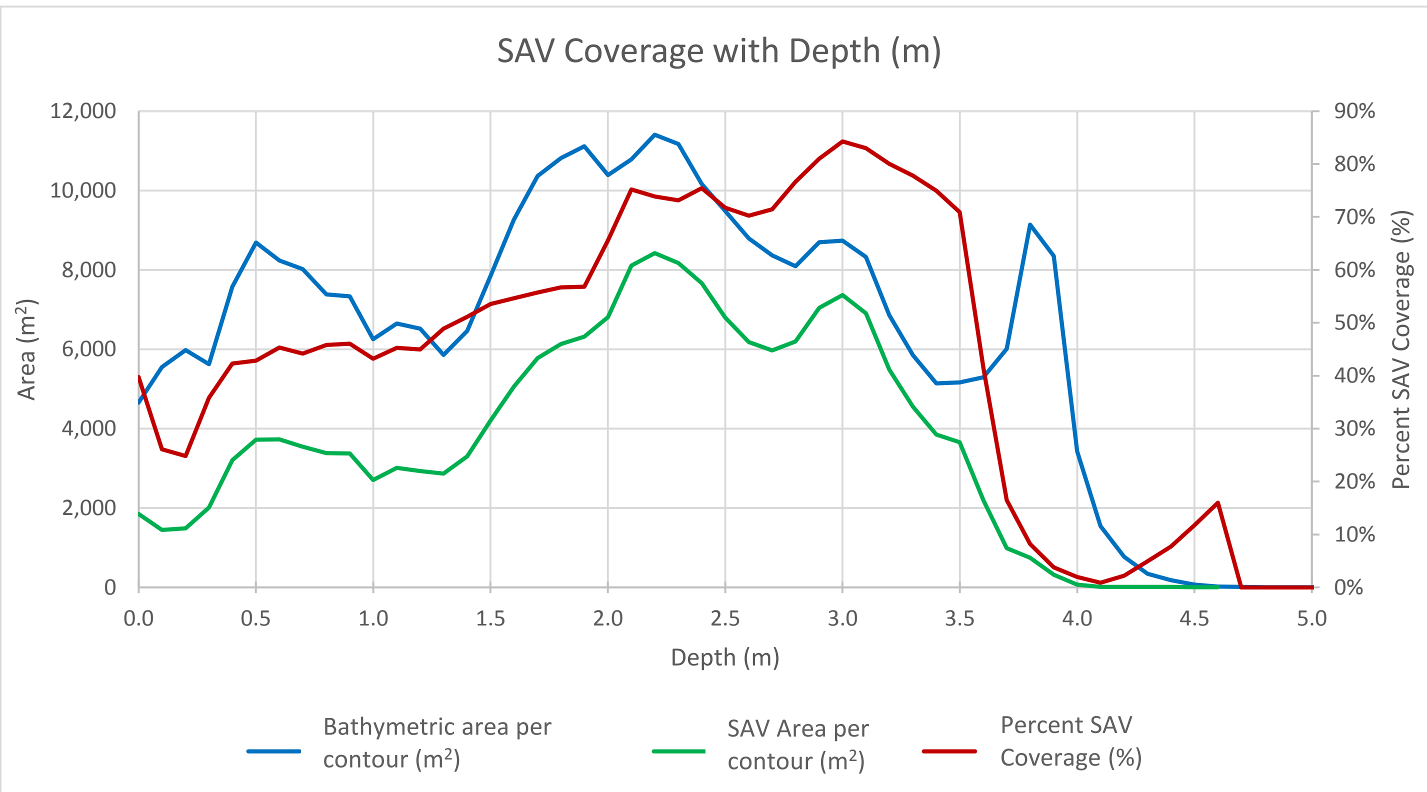

Figure 3.10: Bathymetric area (left axis, blue line) and SAV area (left axis, green line) per 10 cm depth contour, and Percent SAV coverage per depth contour (right axis, red line).

4 Discussion

4.1 Limitations

A limitation of this study was the inability of the laser to penetrate deeper than 4.5 m into the water column. We suspect that there was an area of turbidity in the central, deep part of the lake caused by runoff from the rain event two days prior to the survey on September 22. Given the lake's past history of suspended sediment discussed in the Introduction and Stantec's suggestion that Lake Banook may be acting as a net sink for suspended particulate matter (2014), we believe it is reasonable to assume that turbidity played a role in preventing laser penetration at depth. The bathymetry itself may have limited laser penetration as well. The dredged areas along the eastern shore of the lake near Graham's Grove and along the seawall have very sharp drops in depth; this combined with dark lakebed composed of either weeds or sediments is approaching the limitations of the laser itself. Note that King (2007) indicates the 3 m depth contour marks the beginning of softer, darker, bioturbated muds which would correlate to a lower lidar backscatter value as well.

4.2 Lake Banook Bathymetry

Although the lidar missed the deep areas of the lake, the DEM where it exists is of high resolution and excellent quality and highlights the changes to the lakeshore and bathymetry, especially in the northern part of the lake that has undergone many anthropogenic changes. Figure 4.1 shows bathymetric contours of the lake from the Nova Scotia Department of Fisheries and Aquaculture (NSDFA, 2013), GSC (King, 2007), and our lidar DEM. The exact date of the NSDFA contours is unknown, although it is sometime before the construction of Highway 111 in the early 1990s. We show two shorelines from GSC: from 2007, before the most recent lake modifications, and one estimated to be the shoreline before the lake was flooded for the construction of the Shubenacadie Canal in the 1850s (Huppertz et al., 2008b). The lidar extent represents the 2014 shoreline and it matches the 2007 shoreline well, but the differences with the NSDFA shoreline are vast, highlighting changes to the lake over the past few decades. Figure 4.1A and B show the expansion of Graham's Grove Park with dredged material in preparation for the Canada Games in 1989 , and changes such as infilling in the northern part of Lake Banook where Highway 111 now crosses. The dredged areas are marked by a sharp linear transition along the eastern shore between green and brown. The pre-canal shoreline is of great interest when compared to the lidar, where we see shallow areas corresponding to submerged islands (Figure 4.1C and D). It is also interesting to note the similarity of the pre-canal shoreline and the extent of the lidar in many areas of the lake.

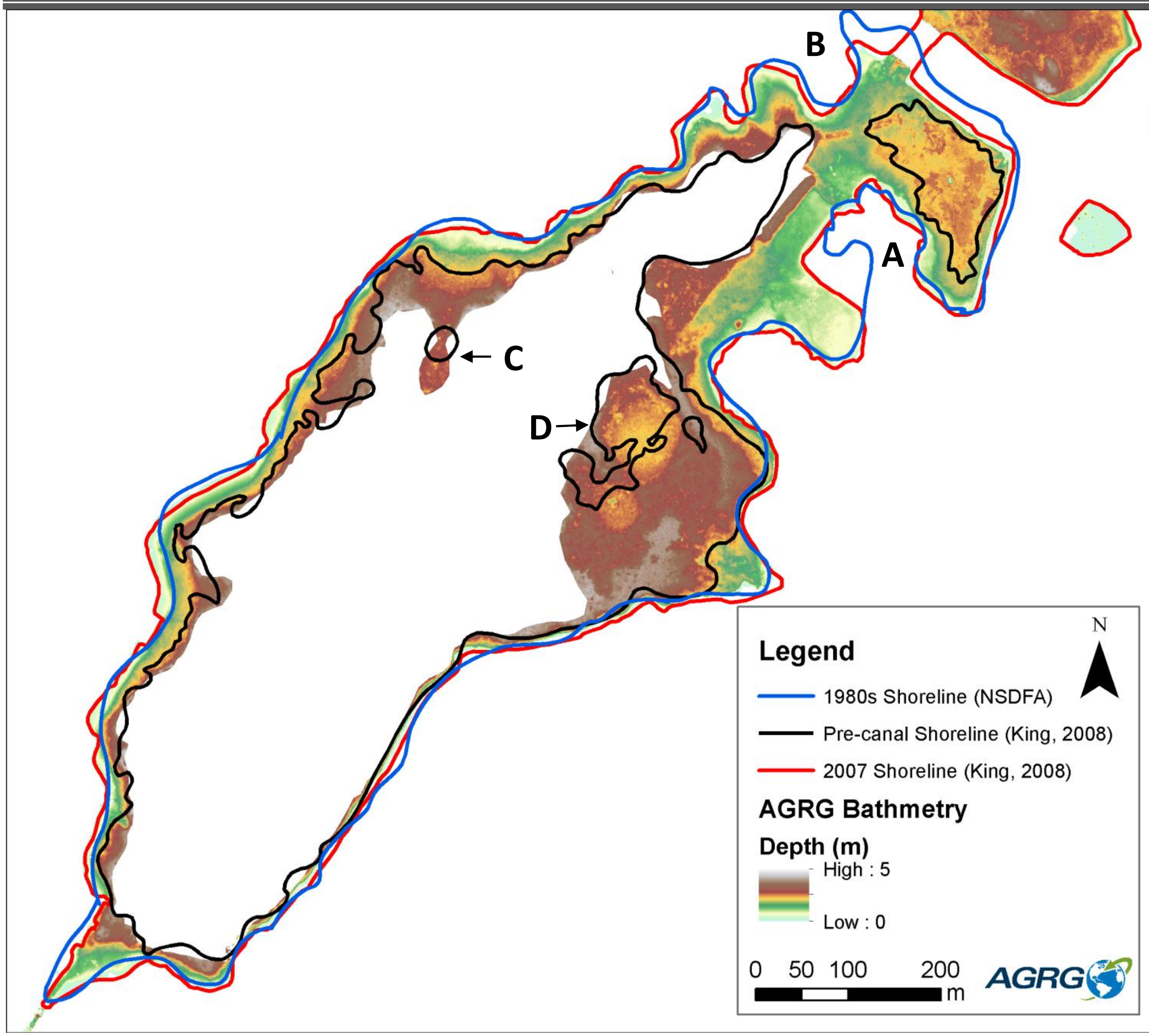

Figure 4.1: Various bathymetric contours for Lake Banook from different time periods. A marks Graham's Grove Park, B marks the bridge at Highway 111, C and D mark submerged islands.

4.3 SAV Distribution

SAV vegetation distribution as detected by bathymetric lidar and aerial photograph analysis indicated plant life abundance increases with depths up to 2 - 3 m and then suddenly drops off at 3.5 - 4 m, just before the limit of the lidar depth penetration. It is of note that the GSC's work done prior to draining the lake in 2008 determined that little to no vegetation existed in the lake at or below 3 meters (King, 2007). They suggest this is due to a combination of growth limiting factors; including the accumulated extinction of light with depth, but also in relation to a physical change in lake bed sediment from cobbled gravels to bioturbated muds (King 2007). Following the lake drain in 2008 Stantec (2014) observed SAV down to 4 – 5 growing in soft and fine grained sediments. Stantec also indicate the lake drawdown as a possible trigger of changes in sediment biogeochemistry that could have caused the redistribution of the plant. Further examination may be prudent to determine with greater confidence whether the SAV detection as presented in report does support the hypothesis that SAV is now (post lake draining) growing consistently at deeper depths , perhaps in different habitat than in 2007; and to what extent darker bioturbated muds are being mis-classified as dark submerged vegetation. It is believed though, that the physical characteristics of this low energy deposited mud layer should be detected as lower signatures in terms of the additional SAV analysis conducted including bed roughness and SAV heights whereas the mud should typically manifest flatter and more featureless than areas of gravel-cobbles.

4.4 Future Work

The methodologies developed for this project will be invaluable for future vegetation classification studies of freshwater or coastal environments. The ability to combine the bathymetric data products with aerial photographs allows great flexibility in determining vegetation presence and gives us the ability to customize the classification approach based on the environment and dataset. It is of note, however, that the reliance of aerial photographs as a mode for classification for SAV does then require special attention be placed on the preparation of such photographs over water bodies such that radiometric consistency can be established. This may require some target placement on and in water bodies for future work for validating photograph radiometry more consistently. Furthermore, common complications when photographing water such as wave reflection and sun glint are more serious an issue when attempting to remove water column radiometric signatures for bottom classification and should be similarly removed more effectively than what is currently done. The depth normalization routine itself, which requires high spatial resolution depth information such as lidar bathymetry, does show great promise for use in classifying submerged environments radiometrically. Methods which allow for accommodating spatially varying water column conditions would benefit the process significantly in addition to other general tweaks to the procedure.

We believe that further customization and classification accuracy can be achieved through the development and integration of algorithms that use the waveform to classify SAV. At this time, lidar backscatter waveforms collected from the Chiroptera II at AGRG have been interpreted into three-dimensional point clouds using a suite of standard tools provided by Leica-AHAB. These tools are designed for function reliably for identifying bottom returns specifically, rather than vegetation. Figure 4.2 shows an example of waveform returns from two different areas of Lake Banook with two different bottom types. We can see that the waveform for the sandy bottom shows two distinct peaks, one representing the water surface and one representing the lake bottom, while the vegetation waveform shows a third response from the water column that represents a return from SAV. The tools currently in use do not allow us to customize the way points are classified from the waveforms to access the middle peak that represents vegetation. Specific waveform interpretation tools for SAV detection is an ongoing field of development at AGRG and tools are being developed to take better advantage of the unique insight into water column features that are captured by lidar and available in the waveform. Some SAV features have been discretized into points which have been classified and used to generate SAV height maps, and further developments of SAV specific waveform interpreters will increase the effect of this approach, perhaps significantly.

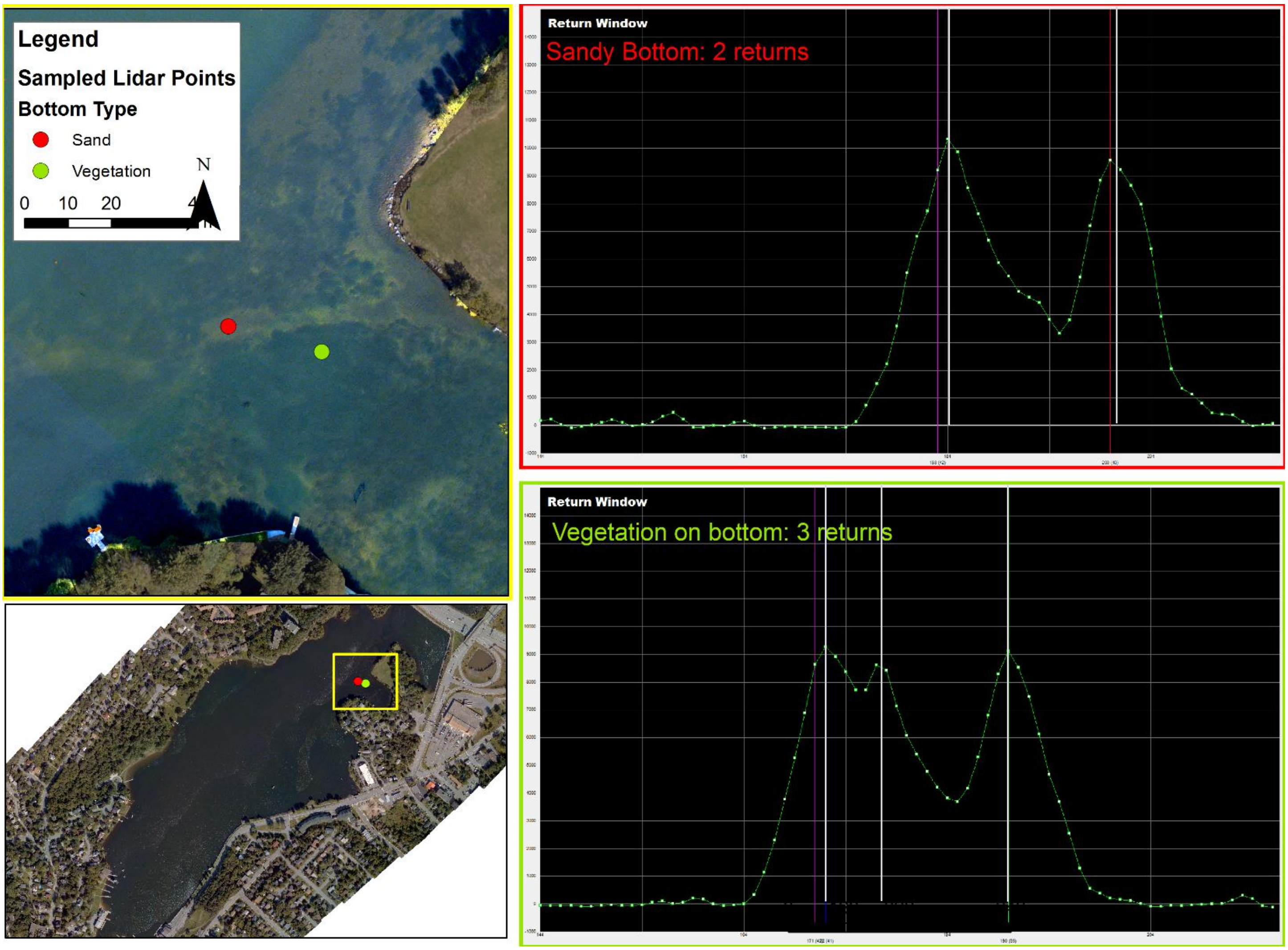

Figure 4.2: An example of waveforms for a sandy bottom type and a vegetated bottom type. The sandy bottom waveform has two peaks (surface and bottom) while the vegetated bottom has an additional peak that represents a return from vegetation.

5 Conclusions

The focus of this study was to test the limitations of the lidar sensor for the application of monitoring SAV distribution and biomass in a lake environment. We developed new and innovative techniques to classify SAV that encompassed multiple components of the data obtained during the aerial survey including the reflectance, aerial photographs, and bathymetry data, and we came up with a map for presence/absence of SAV that agreed very well with our ground truth data. Successful laser penetration was limited to 4.5 m depth by a combination of turbidity and depth itself, which sharply dropped off in many dredged areas of the lake. The SAV map was spatially limited to the areas where laser penetrated to the bottom of the lakebed but within the area of good bathymetric data returns we were able to successfully classify SAV. Our classification agreed well with current ground truth information, and reasonably well with older ground truth data (2007). Our ground truthing data suggested that SAV was not present in the deeper parts of the lake that we were not able to map. Of the area that we classified (32.32 hectares) , 54.9% of the area contained SAV (17.74 hectares) which varied in height from less than 0.1 m to 1.88 m. Further ground truth data is required for future studies to discern the difference between dark sediments at depth and tree shadows near the shoreline, which caused some possible mis-classifications of SAV.

6 Acknowledgements

We graciously thank Ned King of GSC and Don Gordon, formerly of DFO, for their insights into this project; we especially thank Ned King for generously sharing his data.

7 References

Canada Games (2015). 1969 Halifax/Dartmouth Canada Summer Games.

Castell, C. (1977). Results of some studies made on the water of the Dartmouth lakes in 1977 with special emphasis on the amounts of suspended solid material in the water and pH value.

Clement, P., Keizer, P.D., Gordon, D.C.J., Clair, T.A., and Hall, G.E.M. (2007). SYNOPTIC WATER QUALITY SURVEY OF SELECTED HALIFAX REGIONAL MUNICIPALITY LAKES ON 28-29 MARCH 2000 (Dartmouth, NS).

Environment Canada (2015). Daily Data Report for March 2000.

Gordon, D.C.J. (1973). Final report of the water quality study of Lakes Banook and Micmac, summer 1973.

Gordon, D.C.J. (1978). Secchi Disk Observations in Dartmouth's Lakes. 1977.

Gordon, D.C.J., P.D. Keizer, J.G.Ogden III, J. Underwood, and J.F. Wiltshire (1981). Synoptic water quality survey of fifty lakes in the Halifax, N.S. Metro Area on 14 April 1980.

Halifax Regional Municipality (2008). Lake Banook Infrastructure Improvements Get Underway.

Huppertz, T.J., King, E.L., Peters, N.M., and Cameron, G.D.M. (2008a). Geological Setting of Lake Banook- sedimentation and habitat in an urban lake.

Huppertz, T.J., Peters, N.M., King, E.L., and Cameron, G.D.M. (2008b). Glacial and environmental history of Lake Banook, Dartmouth, Nova Scotia, Canada (Dartmouth, NS).

Keizer, P.D., Gordon, D.C.J., T.W. Rowell, R. McCurdy, D. Borgal, T.A. Clair, D. Taylor, J.G.Ogden III, and G.E.M. Hall (1993). Synoptic Water Quality Survey of Halifax/Dartmouth Metro Area Lakes on April 16, 1991.

King, E.L. (2007). Lake Banook Geological Investigations (Geological Survey of Canada).

King, E.L., and Geological Survey of Canada (2008). Gridded multibeam bathymetry, Lake Banook 2007, Dartmouth, Nova Scotia, Canada.

Mosher, D. (2008). Defense Research and Development Canada Atlantic ROV survey of Lake Banook, Dartmouth, NS, Canada. 2007.

Nova Scotia Department of Fisheries and Aquaculture (2013). Lake Inventory Maps.

Stantec (2014). Assessment of Aquatic Vegetation Overgrowth in Lake Banook: Development of Mitigation Alternatives.

World Health Organization Fact Sheet 2.33: Turbidity measurement.

Wyre, L.A. (2006). SUSPENDED SEDIMENT CONCENTRATIONS AND DISAGGREGATED INORGANIC GRAIN SIZES (DIGS) ANALYSIS OF LAKE CHARLES AND LAKE MICMAC DARTMOUTH, NOV A SCOTIA. BSc. Dalhousie University.